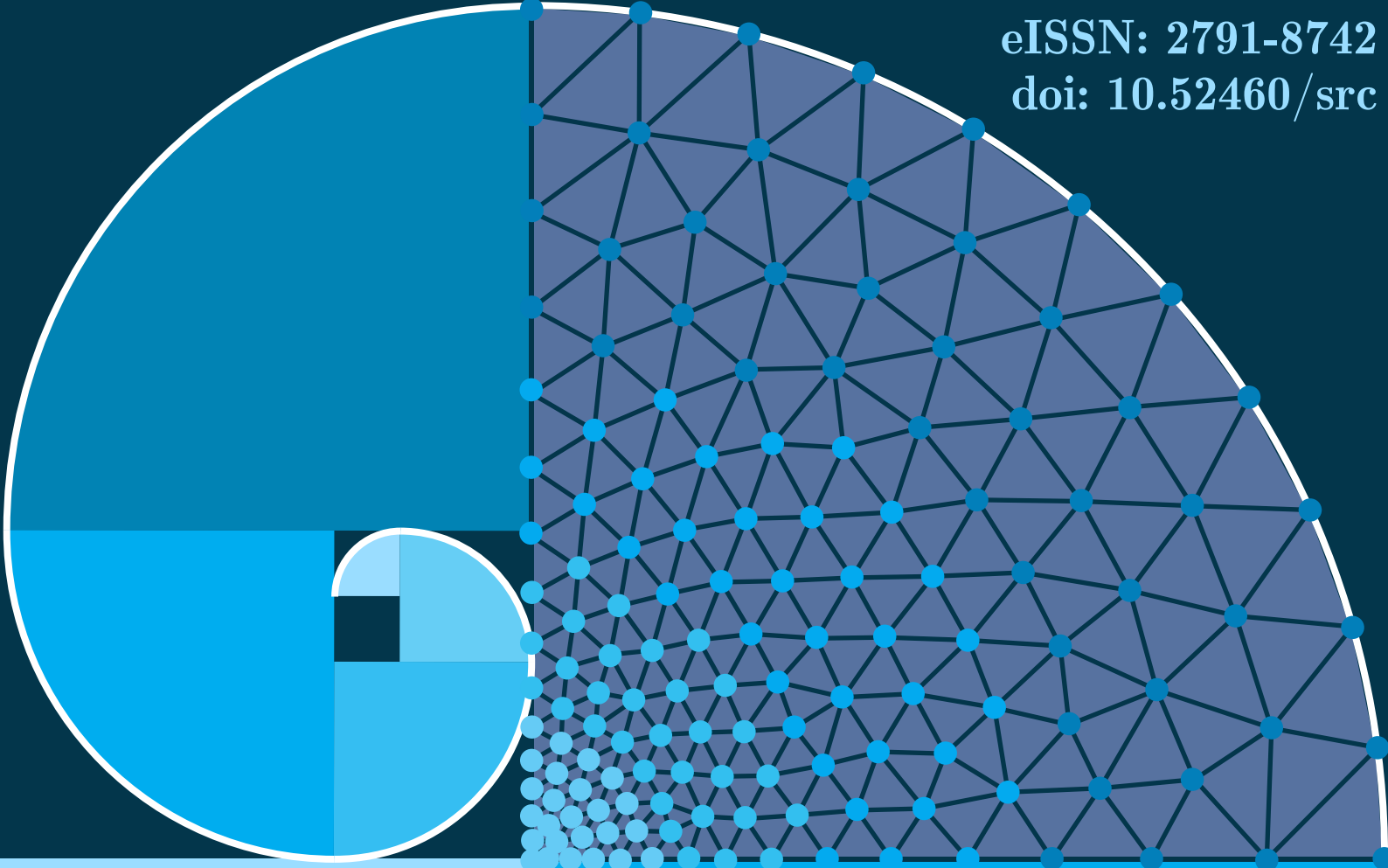
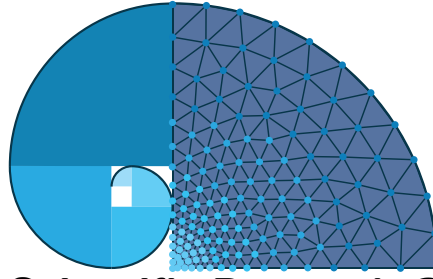


eISSN: 2791-8742
doi: 10.52460/src



**Scientific
Research
Communications**

**Volume 4
Issue 1
January 2024**



Scientific Research Communications

Volume 4, Issue 1, 2024

Editorial

Editor-in-Chief

Mehmet ÇEVİK

Associate Editors

Ahmet AYKAÇ

Aydın AKAN

Ayşe KALAYCI ÖNAÇ

Erman ÜLKER (Guest Editor)

Faruk ÖZGER

Gökçen BOMBAR

Sedat YALÇINKAYA

Sercan ACARER

Umut CEYHAN

Office

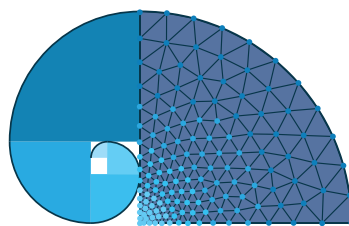
Furkan EMREM

Zehra BÜYÜKER

Publisher

Prof. Dr. Mehmet ÇEVİK

İzmir International Guest Students Association



Scientific Research Communications

Volume 4, Issue 1, 2024

Contents

Implementation of 3ω Method for a Wide Range Measurements of Thermal Conductivity of Liquids, pp.1-11

İ. Ateş and A. Turgut and A. M. Genç and S. Doğanay and L. Çetin

Morphological Analysis of Ksar Tadjrouna in Laghouat, Algeria, pp.12-22

F. I. Mahcar

Application of Inelastic Nonlinear Buckling Analysis with Stiffness Reduction Factors to Web Tapered I Sections, pp.23-34

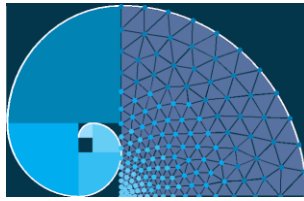
O. Toğay

Innovative Approaches to Modeling Economic Dynamics: Taylor Matrix Methods in Solving Budget Constraint Differential Equations, pp.35-43

N. Baykuş Savaşaneril

An Efficient Index-Based Algorithm for Exact Subgraph Isomorphism on Bipartite Graphs, pp.44-60

M. B. Koca and F. E. Sevilgen



Implementation of 3ω Method for a Wide Range Measurements of Thermal Conductivity of Liquids

İsmet Ateş¹ , Alpaslan Turgut^{2,*} , Alper Mete Genç³ , Serkan Doğanay⁴ , Levent Çetin⁴ 

¹ The Graduate School of Natural and Applied Sciences, Dokuz Eylül University, Izmir, Turkey

² Mechanical Engineering Department, Dokuz Eylül University, Izmir, Turkey

³ The Graduate School of Natural and Applied Sciences, Izmir Kâtip Celebi University, Izmir, Turkey

⁴ Mechatronics Engineering Department, İzmir Kâtip Çelebi University, Izmir, Turkey

* Corresponding author: alpaslan.turgut@deu.edu.tr

Received: 06.09.2023

Accepted: 11.10.2023

Abstract

Thermal conductivity is an important thermophysical property of materials. The advancements in material sciences and manufacturing techniques have led to the development of various techniques for thermal conductivity measurements. Among these methods, the AC hot wire (3ω) method is a prominent option due to its advantages such as insensitivity to black body radiation and minimal sample requirement. Even though this measurement method has been quite popular in thermal conductivity measurements of thin films for several decades and is gathering attention for the measurements of liquids, there are no studies where the hardware of the measurement methodology is depicted as the method is quite complicated. In this study, a custom-made 3ω setup is presented and its performance in a wide range of thermal conductivity measurements is evaluated by investigating the thermal conductivity of base fluids such as water, ethanol, methanol, ethylene glycol (EG), and mineral oil. In addition, the relative thermal conductivity of the base fluids is compared with the literature. The proposed setup shows that the maximum error rates were obtained as in a range of 0.5 to 5% depending on the base fluid.

Keywords: 3ω method; hot wire method; relative thermal conductivity.

1. Introduction

Thermal conductivity is an important thermophysical property of the materials. The advancements in material sciences and manufacturing techniques have led to development of various techniques for thermal conductivity measurements. Among these methods, AC hot wire (3ω) method is a prominent option due to its advantages such as, insensitivity to black body radiation and minimal sample requirement (Cahill, 1990).

In 3ω method, a metal wire, which is used as both a heat source and a thermal sensor, is inserted into the sample. Then, an alternating current is applied at the frequency of ω which results in heat dissipation with 2ω frequency. This periodical input causes a temperature distribution at the same frequency with a phase difference as an output. Due to the temperature dependence resistivity of metals, an oscillating resistance deviation is added to the resistance of the hot wire. Eventually, an observable voltage drop at 3ω is obtained on

sensor terminals. The thermal conductivity of the sample can be obtained by using the amplitude and frequency relationship of 3ω harmonic (Turgut et al., 2008) (Figure 1).

3ω thermal conductivity measurement method has been popular for several decades for the thermal characterization of solids and thin films (Su et al., 2016). Only a few attempts have been made for measurement of fluids in the last two decades (Hoffmann et al., 2016; Karthik et al., 2012; Oh et al., 2008; Turgut et al., 2008; Wang et al., 2007; Wu et al., 2009). Although the reliability of 3ω method is proved experimentally by several research groups, any test device that implements the method is not commercially available.

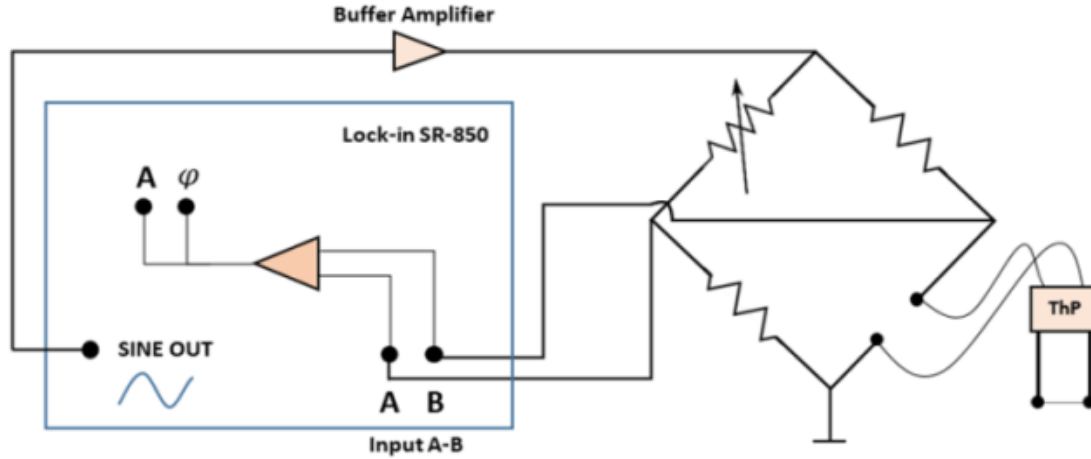


Figure 1. 3ω measurement setup (Turgut et al., 2008)

In this paper, a custom-made electronic hardware for 3ω measurements is presented. The performance of the developed system is investigated in a wide range thermal conductivity measurements of base fluids. The wide range measurement in this study refers to the thermal conductivity change between water (~ 0.6 W/mK) and mineral oil (~ 0.1 W/mK) which calculated as 5 times. The compatible results with previous measurements in the literature for mineral oil (Koruk et al., 2017), water (Çengel & Ghajar, 2014), in addition ethanol, methanol and ethylene glycol samples (Lide, 2004) promise possible use of the developed setup.

2. The 3ω Method

The theoretical background of the 3ω method is briefly explained as they are previously explained in more detail by Turgut et al. (2008) and Chirtoc & Henry (2008). The temperature amplitude $T(2\omega, \phi)$ is given in Eq. (1).

$$T(2\omega, \phi) = \frac{\dot{q}}{2\pi k_s l} \left(\ln \frac{\mu_s}{1.2594r} - i \frac{\pi}{4} \right) \quad (1)$$

where ϕ is the phase angle (radian), \dot{q} is the rate of heat transfer (W), k_s is the thermal conductivity of sample (W/mK), l is half of the length of the wire (m), μ_s is the thermal diffusion length (m), and r is the radius of the wire (m). The second harmonic is obtained by the rate of the heat transfer amplitude. The dimensionless impedance F factor is presented in Eq. (2) (Turgut et al., 2008).

$$F(2\omega) = \frac{Z_s}{Z_p} = \frac{z_s/2\pi r l}{l/(\pi r^2 k_p)} = \frac{k_p r}{2l^2} z_s(2\omega) \quad (2)$$

where z_s ($\text{m}^2\text{K}/\text{W}$) is the specific thermal impedance of the interface, k_p is the thermal conductivity of probe (W/mK), and Z_p is the thermal resistance of the half-length wire in the axial direction, considering the end supports as an infinite heat sink.

The term $V(3\omega, \phi)$ depending on the 3ω is generated by the mixing of excitation current at ω with the resistance change at 2ω and it is given in Eq. (3);

$$V(3\omega, \phi) = \frac{I_0 R_0}{2} r_{el} T(2\omega, \phi) \quad (3)$$

Where I_0 is the current through the wire (A), R_0 is the resistance of wire (Ω), and r_{el} is the temperature coefficient of the resistance ($1/\text{K}$).

With Eq. (1), Eq. (2), Eq. (3) is transformed into Eq. (4);

$$V(3\omega, \phi) = \left(\frac{Il}{\pi r^2} \right)^3 C_M F(2\omega) \quad (4)$$

where I is the current (A) and C_M is the figure of merit. To determinate the relative thermal conductivity, the imaginary parts of Eq. (5) are proportioned for water and the sample. The proportion of the imaginary parts is presented in Eq. (6);

$$V(3\omega, \phi) = \text{Re}(3\omega, \phi) + i\text{Im}(3\omega, \phi) \quad (5)$$

$$\frac{k_s}{k_w} = \frac{\text{Im}[V_w(3\omega, \phi)]}{\text{Im}[V_s(3\omega, \phi)]} \quad (6)$$

where k_w is the thermal conductivity of water (W/mK).

The relationship between the theoretical results and the measurements in the 3ω method is also given in Figure 2 as a block diagram. The developed embedded hardware was designed as three components that are the main controller and signal generator, signal conditioning and lock-in amplifier stages. The components are shown in Figure 3 for performing the measurement of the thermal conductivity of fluids.

Two sinusoidal signals are generated which are synchronous with each other in the setup. One of the generated sinusoidal signals is to excite the probe and the other one is the reference signal needed to perform the measurement. The key principle of measurement method is measuring of 3rd harmonic of modulated sinusoidal wave which is effected with relation between heating wire and excited liquid. In this way, sinusoidal wave at $3f$ frequency is generated as a measurement reference signal. Theoretical and experimental studies have determined that nickel wire probes provide the most appropriate signal (0.5 V amplitude and 0.5-2 Hz frequency range) for measurement (Turgut et al., 2008). In this regards, 1 Hz sinusoidal signals for exciting the probe and 3 Hz sinusoidal signals for the reference are generated in this unit. A 32-bit microcontroller with 12-bit DAC resolution is used to perform this operation.

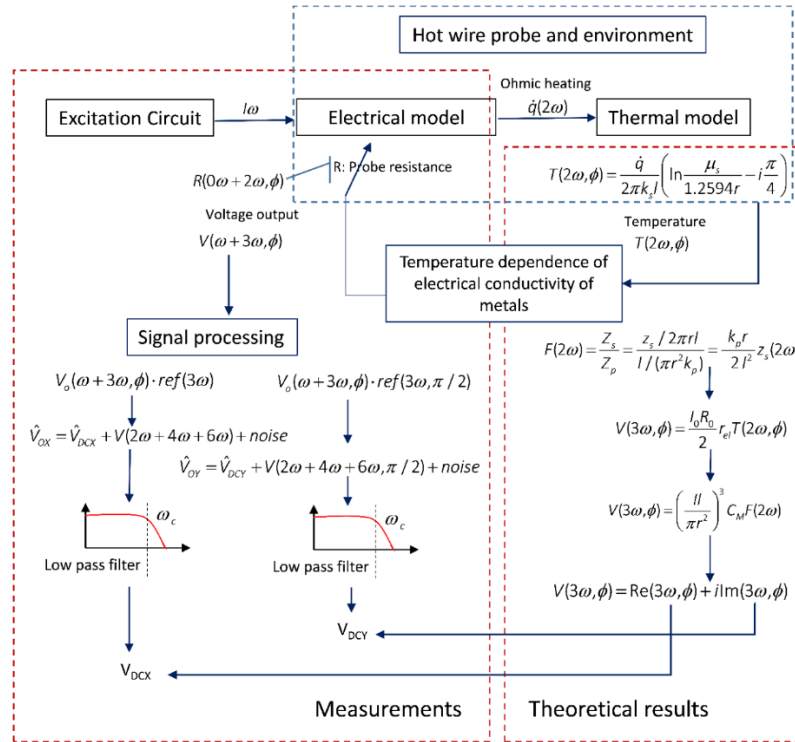


Figure 2. Theoretical and physical explanation of 3ω method

The signals are processed through the 2nd order Butterworth low-pass filters to eliminate switching noise on the digitally generated sinusoidal waves for providing pure sinusoidal signals to lock-in amplifier. Then, the signal is amplified by the preamplifier to provide the required amplitude at the experiment. After that, the signal is amplified by the current amplifier in order to provide sufficient current to excite the wire for sensing temperature change around the wire related with thermal conductivity of the liquid.

The temperature around the probe in the sample form by the effect of the signal, with the resistance of the probe varies proportionally and the Wheatstone bridge is used to detect this change (Figure 1). Since the resistance change affects the voltage balance at the Wheatstone bridge outputs, on both legs of the bridge is sent to the lock-in amplifier for the signal measurement. Before this process, for each measurement output voltage of Wheatstone bridge should be balanced to cancel the ω signal by auto zeroing unit Ateş et al., 2016).

Since the signal difference from the Wheatstone bridge is quite small, this signal is amplified with a gain of 95 dB with the instrumentation amplifier, and then the modulated signal is sent to the lock-in unit. The lock-in amplifier is a measurement device based a phase sensitive detection which developed to detect very small AC signals about a few nanovolts in noise. The signal component at a certain frequency and phase in the signal to be measured by this method can be measured according to the frequency of the reference signal. With this method, undesirable signal components and noises can be filtered better than band pass filters tuned very high Q factor.

In order to detect the 3ω signal, an analog demodulator is used as a phase sensitive detector in the developed system for measurement. The signal modulated with 3 Hz sinusoidal generated due to the heating effect on the 1 Hz carrier signal is multiplied with the reference signal at 3 Hz by the demodulator. The output of the demodulator is the product of four sinusoidal waves and noise. These sinusoidal waves are generated with sum and difference

frequency of signal and reference by multiplication of them. If the frequency of the modulated signal is equal to reference frequency, the output signal will be a DC signal as the frequency difference is zero. If output signal of the demodulator is filtered by 3rd order Butterworth low pass filter, undesired signals and noise rejected thus output signal of the filter is proportional to the modulated sinusoidal wave amplitude as can be seen in Figure 2. The signal at duplicated frequencies are filtered by 3rd order a Butterworth low-pass filter demodulator output. Since the imaginary part ratios are important for thermal conductivity measurement, the phase of the reference signal is shifted by 90 degrees during the measurement process, so that the voltage at the lock-in output directly gives the value of the imager part.

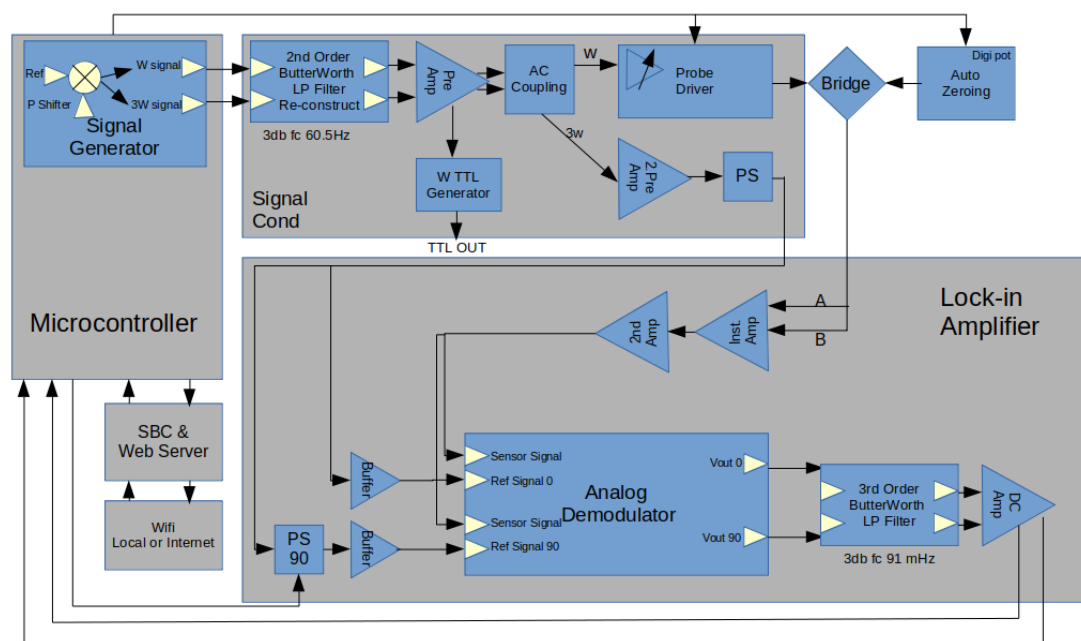


Figure 3. The block diagram of the hardware

Imaginary voltage signal in lock-in amplifier output is logged as a real time at 62 Hz sampling frequency rate by 12-bit ADC of microcontroller. Since the thermal conductivity value is determined to relative, the reference liquid and the sample liquid are measured separately and the data of the each measurement are recorded individually. When the testing process time is ended, embedded software analyze gathered data of two different liquids. The average values are calculated with using intelligent algorithm to finding steady-state arrays. The ratio of the thermal conductivity is calculated relatively by the average obtained values of the sample and the reference liquid.

3. Results and Discussions

The imaginary part of the signal related to the thermal characteristic of the fluid in the measurement process is logged from the output of the lock-in amplifier. The setup is designed as an application specific electronic hardware for providing basic measurement output previously mentioned as the working principle. It is waited for 15 seconds to get the setup reached for the steady state conditions. Then the data is logged for a time period of 64 seconds with totally 500 number of samples.

In order to observe the repeatability and wide range performance of this specifically designed measuring system, the experiments were carried out for the base fluids. In a wide range

measurements, mineral oil (0.120 W/mK) (Koruk et al., 2017) and water (0.598 W/mK) (Cengel & Ghajar, 2014) were chosen as samples. In addition, ethanol (0.169 W/mK), methanol (0.200 W/mK) and ethylene glycol (0.256 W/mK) samples, which have reliable values (Lide, 2004) in the literature, were also used.

When the imaginary voltage values of the measured reference fluid and the sample fluid whose thermal conductivity is to be determined are proportioned according to Eq. 6, thermal conductivity change rates are calculated for each sample depending on the reference fluid. For all samples, water measurement was carried out as a reference sample in accordance with the working systematic and calculations were made according to the voltage values of the water. In order to facilitate traceability, two measurement results representing the general behavior are presented in the graphics. Indices 1 and 2 were used for each measurement result.

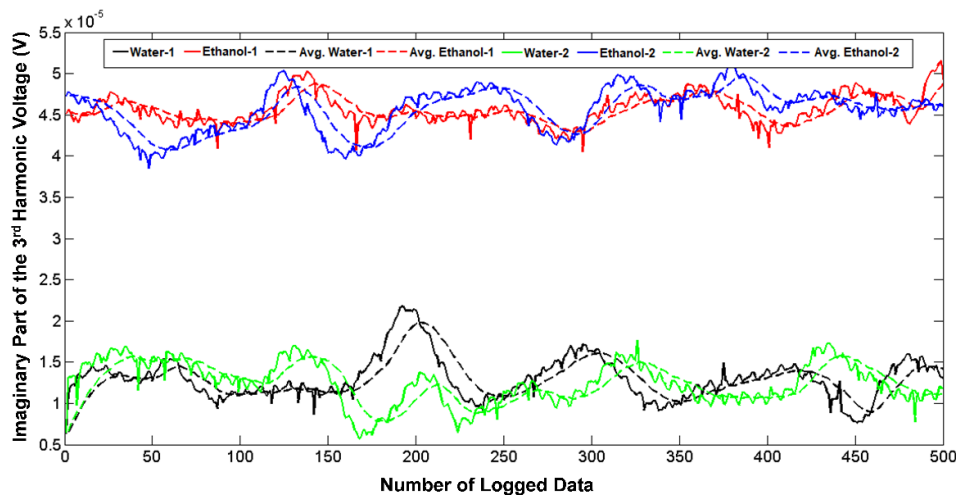


Figure 4. Imaginary part of the voltage signals of the 3rd harmonic of the ethanol sample

In Figure 4, the voltage values obtained for ethanol-1, ethanol-2 and water-1 and water-2 used as reference fluids are shown. The averages of the voltage values obtained were calculated as 45.575 and 45.582 μV for ethanol-1 and ethanol-2, respectively, and 12.802 and 12.339 μV for water-1 and water-2, respectively. When the acquired voltage values are proportioned according to the expression in Eq. 6, the relative thermal conductivity values for ethanol-1 and ethanol-2 were calculated as 0.281 and 0.271, respectively. Relative thermal conductivity is obtained as 0.275 when literature values of ethanol and water are used. Accordingly, it is seen that the relative thermal conductivity measurements for ethanol-1 and ethanol-2 can be measured with a maximum error of $\pm 2.2\%$. Voltage values for methanol, ethylene glycol (EG), and mineral oil samples are shown in Figure 5, Figure 6, and Figure 7, respectively.

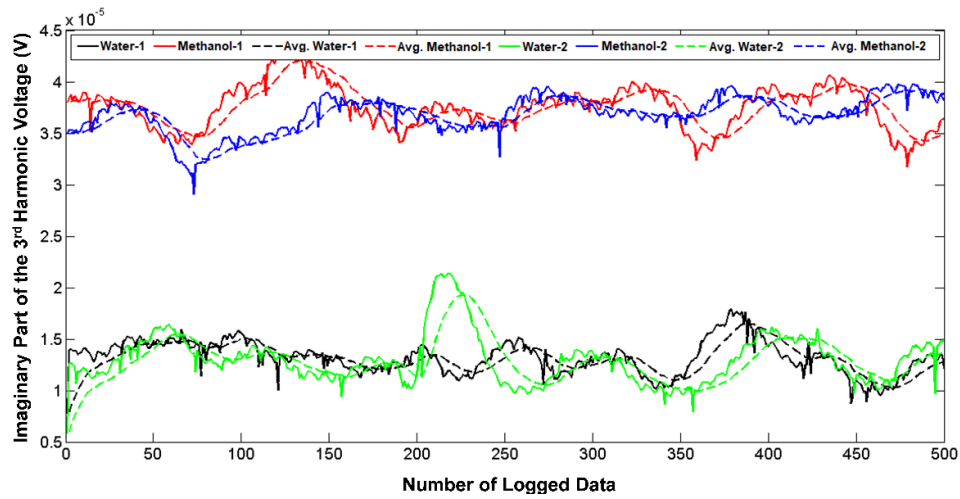


Figure 5. Imaginary part voltage signals of the 3rd harmonic of the methanol sample

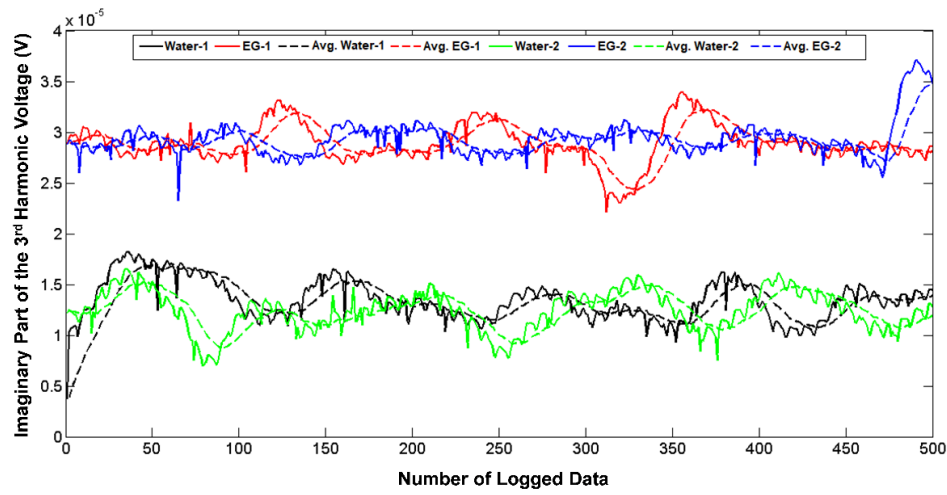


Figure 6. Imaginary part voltage signals of the 3rd harmonic of the ethylene glycol (EG) sample

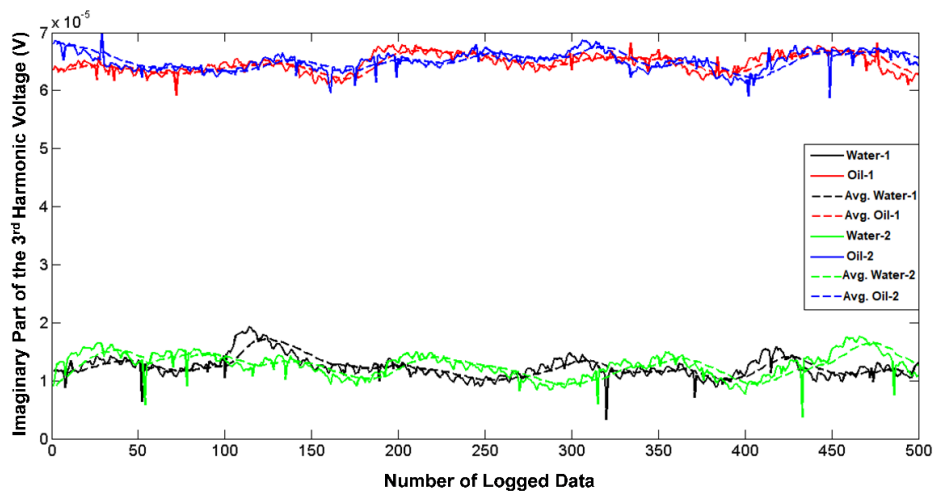


Figure 7. Imaginary part voltage signals of the 3rd harmonic of the mineral oil sample

According to the acquired voltage values, the average voltage values for each sample are given in Table 1. The relative thermal conductivity values calculated based on the average voltage values and their error rates according to the literature values are presented in Table 2.

Table 1. Average values of voltages for samples of wide range measurement

Sample	Average Voltage (μV)
Ethanol-1	45.575
Water-1	12.802
Ethanol-2	45.582
Water-2	12.339
Methanol-1	37.595
Water-1	13.071
Methanol-2	36.725
Water-2	12.793
EG-1	29.182
Water-1	12.370
EG-2	29.349
Water-2	12.505
Mineral Oil-1	64.706
Water-1	12.278
Mineral Oil-2	65.115
Water-2	12.551

As seen in Table 2, the highest error rate in the measurement results for ethanol, methanol, ethylene glycol and mineral oil samples was found in mineral oil with 5%. In methanol and ethylene glycol, the highest error rates were obtained as 3.9% and 0.5%, respectively. It is stated that the results obtained for the ethylene glycol sample are very close to the literature values. According to the obtained relative thermal conductivity results, it is seen that the wide range thermal conductivity measurement performance of the developed system gives results that are quite consistent with the literature.

Table 2. Thermal conductivity ratios for wide range measurement samples

Sample	Relative Thermal Conductivity (Measurements)		Relative Thermal Conductivity (Literature)	Error (%)	
	Min	Max	Average	Min	Max
Ethanol ¹	0.271	0.281	0.275	-1.455	2.182
Methanol ¹	0.348	0.348	0.335	3.881	3.881
EG ¹	0.424	0.426	0.426	-0.470	0.000
Mineral Oil ²	0.190	0.193	0.200	-5.000	-3.500

¹(Lide, 2004), ²(Koruk et al., 2017)

4. Conclusions

In this study, a custom-made electronic hardware for 3ω measurements was presented. The performance of the developed system was investigated in wide-range thermal conductivity measurement of base fluids. In wide range measurements, mineral oil and water, which have approximately 5 times difference between thermal conductivity values, were used as reference

samples. In addition, ethanol, methanol, and ethylene glycol samples, which have reliable thermal conductivity values in the literature, were also measured.

Following conclusions can be drawn from this study:

- ❖ By the improved algorithm, the thermal conductivity ratio of the samples are determined automatically and faster in comparison with Turgut et al., (2008).
- ❖ The developed hardware in this system decreases the essential time to achieve steady state condition.
- ❖ Thermal conductivity results of the base fluids are obtained by the designed system shows a good agreement with the results for mineral oil, water, in addition ethanol, methanol and ethylene glycol samples.
- ❖ The thermal conductivity of base fluids can be measured with a maximum 5% error in the wide range measurement.

Acknowledgments

This work has been supported by TÜBİTAK Project No: 115M408.

Author Statement

The authors confirm contribution to the paper as follows:

Study conception and design: İsmet Ateş, Alpaslan Turgut, Levent Çetin; data collection: İsmet Ateş, Alper Mete Genç; analysis and interpretation of results: İsmet Ateş, Alpaslan Turgut, Serkan Doğanay; draft manuscript preparation: İsmet Ateş, Alper Mete Genç. All authors reviewed the results and approved the final version of the manuscript.

Conflict of Interest

The authors declare no conflict of interest.

Nomenclature

\emptyset	Phase angle (radian)
C_M	Figure of merit
F	Dimensionless impedance
f	Frequency (Hz)
I	Current (A)
I_0	Current through wire (A)
k	Thermal conductivity (W/mK)
k_p	Thermal conductivity of probe (W/mK)
k_s	Thermal conductivity of sample (W/mK)
k_w	Thermal conductivity of water (W/mK)
l	Length of the wire (m)
q	Rate of heat transfer (W)
r	Radius of the wire (m)
r_{el}	Temperature coefficient of the resistance (1/K)
R_0	Resistance of wire (Ω)
T	Temperature (K)
V	Voltage (V)
V_{DCX}	Real part of voltage of 3 rd harmonic (V)
V_{DCY}	Imaginary part of voltage of 3 rd harmonic (V)

V_{0X}	Real part of the voltage (V)
V_{0Y}	Imaginary part of the voltage (V)
Z_p	The thermal resistance of the half-length wire ($m^2 K/W$)
Z_s	The thermal impedance of the interface ($m^2 K/W$)
z_s	Thermal impedance ($m^2 K/W$)
μ_s	The thermal diffusion length (m)
ω	Omega (rad/s)

References

- Ateş, İ., Turgut, A., Çetin, L., Chirtoc, M., & Ieee. (2016). Three omega Probe with Auto-zeroing. 2016 Ieee 22nd International Symposium for Design and Technology and Electronic Packaging (Siitme), 63-65.
- Cahill, D. G. (1990). Thermal-Conductivity Measurement from 30-K to 750-K - The 3-Omega Method. *Review of Scientific Instruments*, 61(2), 802-808. doi:10.1063/1.1141498
- Çengel, Y. A., & Ghajar, A. J. (2014). *Heat and Mass Transfer: Fundamentals and Applications*.
- Chirtoc, M., & Henry, J. F. (2008). 3 Omega Hot Wire Method for Micro-Heat Transfer Measurements: From Anemometry to Scanning Thermal Microscopy (STHM). *European Physical Journal-Special Topics*, 153, 343-348. doi:10.1140/epjst/e2008-00458-8
- Hoffmann, J. F., Henry, J. F., Vaitilingom, G., Olives, R., Chirtoc, M., Caron, D., & Py, X. (2016). Temperature Dependence of Thermal Conductivity of Vegetable Oils For Use in Concentrated Solar Power Plants, Measured By 3 Omega Hot Wire Method. *International Journal of Thermal Sciences*, 107, 105-110. doi:10.1016/j.ijthermalsci.2016.04.002
- Karthik, R., Nagarajan, R. H., Raja, B., & Damodharan, P. (2012). Thermal Conductivity of CuO-DI Water Nanofluids Using 3-Omega Measurement Technique in A Suspended Micro-Wire. *Experimental Thermal and Fluid Science*, 40, 1-9. doi:10.1016/j.expthermflusci.2012.01.006
- Koruk, M., Turgut, A., & Alasli, A. (2017). Evaluating the Thermal Conductivity and Viscosity of CuO-Nanolubricants. *Key Engineering Materials*, 750, 159-163. doi:10.4028/www.scientific.net/KEM.750.159
- Lide, D. R. (2004). *CRC Handbook of Chemistry and Physics* (Vol. 85): CRC press.
- Oh, D. W., Jain, A., Eaton, J. K., Goodson, K. E., & Lee, J. S. (2008). Thermal Conductivity Measurement and Sedimentation Detection of Aluminum Oxide Nanofluids by Using The 3 Omega Method. *International Journal of Heat and Fluid Flow*, 29(5), 1456-1461. doi:10.1016/j.ijheatfluidflow.2008.04.007
- Su, J. W., Liu, X., Charmchi, M., & Sun, H. W. (2016). Experimental and Numerical Study of Anisotropic Thermal Conductivity of Magnetically Aligned PDMS/Ni Particle Composites. *International Journal of Heat and Mass Transfer*, 97, 645-652. doi:10.1016/j.ijheatmasstransfer.2016.02.023
- Turgut, A., Sauter, C., Chirtoc, M., Henry, J. F., Tavman, S., Tavman, I., & Pelzl, J. (2008). AC Hot Wire Measurement of Thermophysical Properties of Nanofluids with 3 Omega Method. *European Physical Journal-Special Topics*, 153, 349-352. doi:10.1140/epjst/e2008-00459-7

- Wang, Z. L., Tang, D. W., Liu, S., Zheng, X. H., & Araki, N. (2007). Thermal-conductivity and Thermal-diffusivity Measurements of Nanofluids by 3 Omega Method and Mechanism Analysis of Heat Transport. *International Journal of Thermophysics*, 28(4), 1255-1268. doi:10.1007/s10765-007-0254-3
- Wu, G. S., Yang, J. K., Ge, S. L., Wang, Y. J., Chen, M. H., & Chen, Y. F. (2009). Thermal Conductivity Measurement for Carbon-Nanotube Suspensions with 3 Omega Method. *Micro and Nano Technology: 1st International Conference of Chinese Society of Micro/Nano Technology(Csmnt)*, 60-61, 394-398. doi:10.4028/www.scientific.net/AMR.60-61.394
- Zhao, D. L., Qian, X., Gu, X. K., Jajja, S. A., & Yang, R. G. (2016). Measurement Techniques for Thermal Conductivity and Interfacial Thermal Conductance of Bulk and Thin Film Materials. *Journal of Electronic Packaging*, 138(4), 19. doi:10.1115/1.4034605

Morphological Analysis of Ksar Tadjrouna in Laghouat, Algeria

Fatiha Imane Mahcar^{1,*} 

¹ Department of Architecture, Faculty of Architecture, Bursa Uludağ University, Türkiye

*Corresponding author: mouniimy6@gmail.com

Received: 06.04.2023

Accepted: 15.01.2024

Abstract

This study focuses on the morphological analysis of Ksar Tadjrouna in Laghouat, Algeria, recognizing the significance of preserving and enhancing the heritage of the region. Emphasizing the broader definition of heritage by UNESCO, the research extends beyond monuments to encompass the cores and historic districts of cities, reflecting cultural, architectural, and historical values. The study explores the traditional architectural form known as "ksar," prevalent in North African fortified villages. In the case of Ksar Tadjrouna, the morphological analysis reveals key characteristics, such as hierarchical plot systems, orthogonal street encounters, planar built structures with central courtyards, and a clear division between public and private spaces. The study identifies pathologies in the Ksar, including the use of heterogeneous materials and degradation issues, leading to a proposed intervention strategy. The proposed plan aims to protect Ksar Tadjrouna by addressing its morphological aspects and enhancing its tourist potential, catering to both national and international tourists through cultural tourism initiatives. The research concludes by emphasizing the importance of morphological analysis for understanding urban fabric changes over time and designing place-centered interventions that contribute to heritage conservation and community continuity. The ultimate goal is to secure the classification of Ksar Tadjrouna as a safeguarded sector, ensuring its preservation as a testament to a rich and distinctive civilization.

Keywords: Morphological analysis, traditional architecture, Ksar of Tadjrouna, laghouat, Algeria

1. Introduction

Algeria is endowed with a very significant heritage, reflecting the influence of various civilizations and cultures. The conservation and enhancement of this heritage constitute one of the main challenges in the practice of architectural preservation. Currently, Algeria, like all countries worldwide, is faced with a phenomenon of demographic growth accompanied by economic development, which has caused excessive urban sprawl characterized by standardized architecture, causing neglect and abandonment of the old districts of cities. This has created the problem of abandonment, marginalization and degradation of this heritage. The Ksar of Tadjrouna in Laghouat, Algeria is one of the 5 Ksours of Laghouat (located on an archaeological site) which is characterized by its richness of urban fabric. Also, it is characterized by its seniority which allows us to take it as a conceptual landmark of traditional architecture.

According to UNESCO, established in 1997, heritage is the common heritage of a nation, or even of humanity: "The cultural and natural heritage is among the priceless and irreplaceable assets, not only of each nation, but of humanity as a whole." (UNESCO, 2019). Algeria has a very important heritage, reflecting the passage of several civilizations and interior cultures, their conservation and enhancement is one of the main issues and concerns of the practice of architectural preservation.

This study is not only interested in monuments and historic sites but also encompasses the cores and historic districts of cities which reflect cultural, architectural and historical values of society.

This heritage, in the context of various experiences, must be approached as a whole, embracing its diversity. "It is the living memory, symbol of a popular culture with strong meanings, which crosses the architectural quality of the buildings and places as well as the urban harmony of the fabric." (Hamma, 2011). Despite the climate, and the arid and challenging nature of the Algerian desert, which occupies four-fifths of the country's total surface area, populations have chosen to settle, live, and adapt in this aggressive environment. These populations have invented all their genius to create human settlements which can protect them against the annoying factors of this region, these establishments are known under the name of "ksour", they are the product of a culture and a set of moral values, they are characterized by a typical architecture. (Brik and Smaali, 2016).

A "ksar" refers to a traditional North African fortified village, predominantly found in countries like Algeria, Morocco, Tunisia, and parts of Libya, with a concentration in desert regions like the Maghreb. These settlements are marked by their unique architecture and layout, strategically designed to offer protection against harsh weather conditions and potential invasions. Ksars are tightly packed communities featuring defensive walls, including towers, constructed from locally available materials like mud bricks. The layout comprises narrow streets and alleys that enhance defense and control temperatures. Central mosques serve as focal points for religious and communal activities, and storage facilities, such as granaries, are integrated to safeguard food supplies in the challenging desert climate. Overall, ksars offer insights into the traditional life of North African communities and the adaptive strategies employed to thrive in their environments (Dłużewska and Dłużewski, 2017).

Currently the urban centers of Algerian cities (like: M'Zab valley in Ghardaia; south of Algeria) are in decline, faced with the difficulties of their conservation and their integration into the contemporary city. It is transformed at the pace and in the image of the populations and activities that mark the dynamism. This is the case, and even more so, with the initial core of all cities, which has a rich past and carries a future which must be able to bear witness to its history, be part of the present and integrate finally these monuments to their future. Moreover, there lies the interest and the challenge of revitalization and enhancement interventions: safeguarding the architectural and urban built heritage without slowing down development" (Hamma, 2011). This phenomenon bears the interest of the degradation of urban heritage in Algeria and the need for its safeguard by our study of the Ksar Tadjrouna in Laghouat which is an example that requires conservation and enhancement operations (Mazouz, 2015).

The "intangible cultural heritage" means the practices, representations, expressions, knowledge, skills – as well as the instruments, objects, artefacts and cultural spaces associated therewith – that communities, groups and, in some cases, individuals recognize as part of their cultural heritage. This intangible cultural heritage, transmitted from generation to generation, is constantly recreated by communities and groups in response to their environment, their interaction with nature and their history, and provides them with a sense

of identity and continuity, thus promoting respect for cultural diversity and human creativity. For the purposes of this Convention, consideration will be given solely to such intangible cultural heritage as is compatible with existing international human rights instruments, as well as with the requirements of mutual respect among communities, groups and individuals, and of sustainable development (UNESCO, 2003).

The “intangible cultural heritage”, as defined in paragraph 1 above, is manifested inter alia in the following domains:

- (a) oral traditions and expressions, including language as a vehicle of the intangible cultural heritage;
- (b) performing arts;
- (c) social practices, rituals and festive events;
- (d) knowledge and practices concerning nature and the universe;
- (e) traditional craftsmanship (UNESCO, 2003).

The UNESCO World Heritage Convention defines (tangible) cultural heritage as:

Monuments: architectural works, works of monumental sculpture and painting, elements or structures of an archaeological nature, inscriptions, cave dwellings and combinations of features, which are of outstanding universal value from the point of view of history, art or science;

Groups of buildings: groups of separate or connected buildings which, because of their architecture, their homogeneity or their place in the landscape, are of outstanding universal value from the point of view of history, art or science;

Sites: works of man or the combined works of nature and man, and areas including archaeological sites which are of outstanding universal value from the historical, aesthetic, ethnological or anthropological point of view (UNESCO, 2003).

Some definitions of interventions:

Conservation means all the processes of looking after a place so as to retain its cultural significance.

Maintenance means the continuous protective care of a place, and its setting.

Maintenance is to be distinguished from repair which involves restoration or reconstruction.

Preservation means maintaining a place in its existing state and retarding deterioration.

Restoration means returning a place to a known earlier state by removing accretions or by reassembling existing elements without the introduction of new material.

Reconstruction means returning a place to a known earlier state and is distinguished from restoration by the introduction of new material.

Adaptation means changing a place to suit the existing use or a proposed use (The Burra Charter, 2013).

The objective of our study is to attempt for the protection of the urban heritage in Algeria from degradation and the need for its safeguard by the morphological analysis of Ksar Tadjrouna in Laghouat which is an example which requires operations of conservation and preservation.

2. Materials and Methodology

2.1. Study Area

The town of Laghouat is located in the Saharan region of Algeria and shares its limits with two towns of the highlands (Tiaret and Djelfa) and two others of the South which are (El Bayadh and Ghardaia) (Figure 1). So, the town of Laghouat constitutes an open door to the great south. It is located at: 410 km from Algiers (capital); 103 km from Djelfa 187 km from Ghardaia, 270 km from Tiaret and 230 km from El Bayadh (PPMVSA, 2018). The town experiences a desert climate with extremely hot temperatures, especially during the summer months. Laghouat has historical importance, and like many towns in the region, it has been influenced by various cultures and civilizations over the centuries. With origins dating back to at least the 11th century, Laghouat was under Ottoman Turkish rule in 1786 and later became part of the Beylik of Titteri (Médéa). The town endured the harsh Siege of Laghouat in 1852 and remained under French colonial administration until 1962. The local economy is often tied to activities related to the surrounding desert, including agriculture, trade, and tourism.



Figure 1. The location of Laghouat (Anonymous, 2020)

Laghouat has architectural and cultural elements that reflect the traditions and heritage of the Saharan region. The town attracts tourists interested in exploring the unique Saharan landscapes, as well as those interested in historical and cultural aspects of the region.

The town of Tadjrouna is located in the southwest of Laghouat province (82 km from Laghouat) (Figure 2). It has a population less than 5000. The ksar is located in the southeast of Tadjrouna city (Direction De La Culture De Laghouat., 2017).

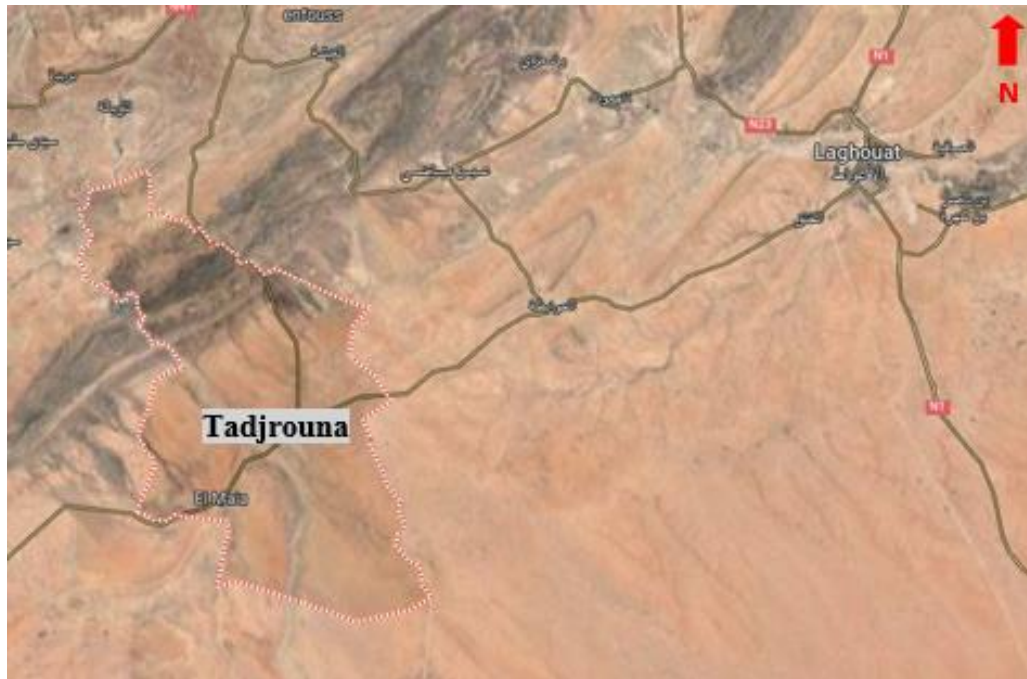


Figure 2. The location of Tadjrouna

2.2. Research Methodology

Urban morphology encompasses various disciplines and is of interest to diverse professions, including architecture, archaeology, anthropology, ethnography, geography, history, and philosophy. It is a branch of urban studies that deals with the form and structure of a settlement. It studies complex and intricate types of forms and how different factors set their mark upon the whole city. In this way urban morphology examines the configuration of the urban form as well as the relationship between the individual forms and the city as a whole, from the formative years of the city through its subsequent transformations (Kristjánsdóttir, 2019). Scheer (2017) defines urban morphology as the examination of the evolving structure of settlements and the analysis of form specifically in terms of physical elements, without delving into the multitude of relationships these elements may have with other attributes or qualities, like livability. Prokopska (2001) applied the morphological analysis technique to architectural designs. Li and Hu (2022) investigated the correlation between the architectural morphology in both 2D and 3D dimensions and the land surface temperature of urban areas, employing a boosted regression tree method, with Beijing, China as a case study. Cömert (2013) aimed to analyze and compare the urban morphological character of medieval-originated towns across diverse geographies and cultures throughout history, investigating the reasons behind the evolution of town morphology over time and understanding how it is shaped within this dynamic process. Can and Heath (2016) conducted a morphological analysis of Izmir through the application of space syntax. This study addresses the intermediate spaces between buildings and streets, exploring the significance and definition

of spatial configuration in connection with urban morphology and social relations. Topçu and Kubat (2012) examined the morphological transformation of Antakya, focusing on spatial integration and making comparisons between the traditional and modern centers of the city.

There are other studies using this methodology. Brzezicki (2021) conducted a morphological analysis of façades with adaptive shading systems, focusing on the spatial relationship between the shading system and the building's glass envelope. Their empirical evidence revealed that the location of the shading system in relation to the building's glass envelope is a crucial morphological feature determining the extent of spatial transformation in the architectural structure where such a system is installed. Wang et al. (2020) applied a framework for digitally describing and generating block forms, emphasizing the morphological complexity of urban blocks. By incorporating design factors such as the environment, transportation, and visibility, and by summarizing the objectives of blocks and buildings into corresponding functions and control indices, the initial generation plan was formulated. Recently Goodarzi et al. (2023) performed a morphological analysis of Persian historical gardens based on cultural DNA concept.

The morphological approach is defined as a tool for understanding traditional fabrics in a clear and explicit way the complexity of the morphological relationships that reign in old neighborhoods through two modes. These are the mode of distribution (parcel and street system) and the mode of occupation (built and open spaces system) (Borie and Denieul, 1984). The processes of this approach are presented (Figure 3).

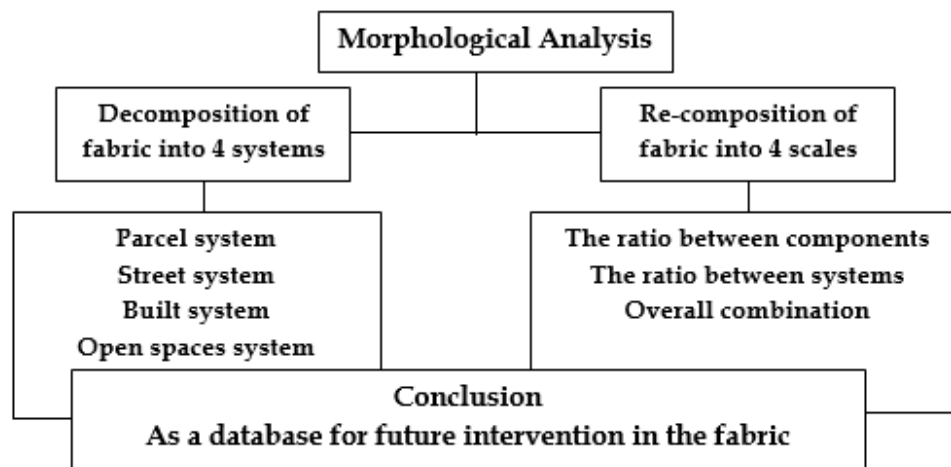


Figure 3. The processes of morphological analysis

The morphological analysis of Ksar Tadjrouna relies to understand how the Ksar has changed in the past and how it may change in the future even without a formal plan. Just as importantly, morphological analysis provides a basis for design that is unique and place-centered. It can protect valuable vernacular resources (e.g. buildings, alleys, street patterns) by recognizing their active contribution to the physical character of the place.

3. Results and Discussion

3.1. Morphological Analysis of Ksar Tadjrouna

Among the traditional fabrics we have our case study; it is the Ksar Tadjrouna which is characterized by its seniority which allows us to take it as a conceptual landmark of traditional architecture. The morphological analysis of Ksar Tadjrouna is shown in Table 1 and Table 2.

Table 1. The decomposition of Ksar Tadjrouna

Decomposition			
Parcel System	Street System	Built System	Open Spaces System
<ul style="list-style-type: none"> ▪ Directions of parcels are hierarchical; this means that a preferential direction ▪ Directions of the plots: The fundamental directions of the plot are mainly linked to a natural limit (valley). ▪ A variant of plots of different dimensions. 	<ul style="list-style-type: none"> ▪ Orthogonal Encounter: the hierarchy of the streets does not modify the frontal continuity of the space prevails on the lateral side. ▪ Inclusion of linear system with loop system (hierarchical). 	<ul style="list-style-type: none"> ▪ Planar built: the buildings are attached to each other on all sides to form a continuous mass. ▪ No ramified planar built. ▪ The type of volumes: building with a central courtyard. 	<ul style="list-style-type: none"> ▪ Planar Building: The differentiation between private free space and public free space tends to be done automatically. ▪ A certain balance between the full and the empty.

Table 2. The re-composition of Ksar Tadjrouna

Re-composition		
Topological ratio between systems	The ratio between the 4 systems	The ratio between systems
<ul style="list-style-type: none"> ▪ Hierarchical plot: is characterized by a hierarchy between the main road and secondary streets. ▪ The plot has a rectangular proportion. 	<ul style="list-style-type: none"> ▪ The free space is very clearly subdivided into a public zone (P) and a private zone (p), in this case the private space is isolated from all sides. 	<ul style="list-style-type: none"> ▪ After the combination between the built system and the street system, we obtain the tissues of: <ul style="list-style-type: none"> * Planar built system - linear street with hierarchized plot. * We have the case of building aligned on the street.

After this morphological analysis, we can emerge the characteristics that present the identity of Ksar Tadjrouna (Figure 4) which must be taken into account in each intervention:

- The fabric characterized by a no ramified planar built.
- Introverted architecture with the courtyard in the house as the basic unit.
- Hierarchical street system from public to private (street, alley and blind alley).
- The blind alley is 3m and 7m for the commercial street.
- The template is limited in between (ground floor to the first floor).

The notion of privacy presented by:

- The use of a public to private crossing space provided by the places.
- The arrangement of the entrance doors in relation to each other.

- Simple facades characterized by treatment of the doors or windows.

This study has allowed us to understand the elements that help the success of the interventions and to put certain parameters considered as reference elements and basic principles for the operations on the Ksar. It also highlights that the revaluation of the Ksar is a very large operation and proposes interventions that allow the preservation of the Ksar.

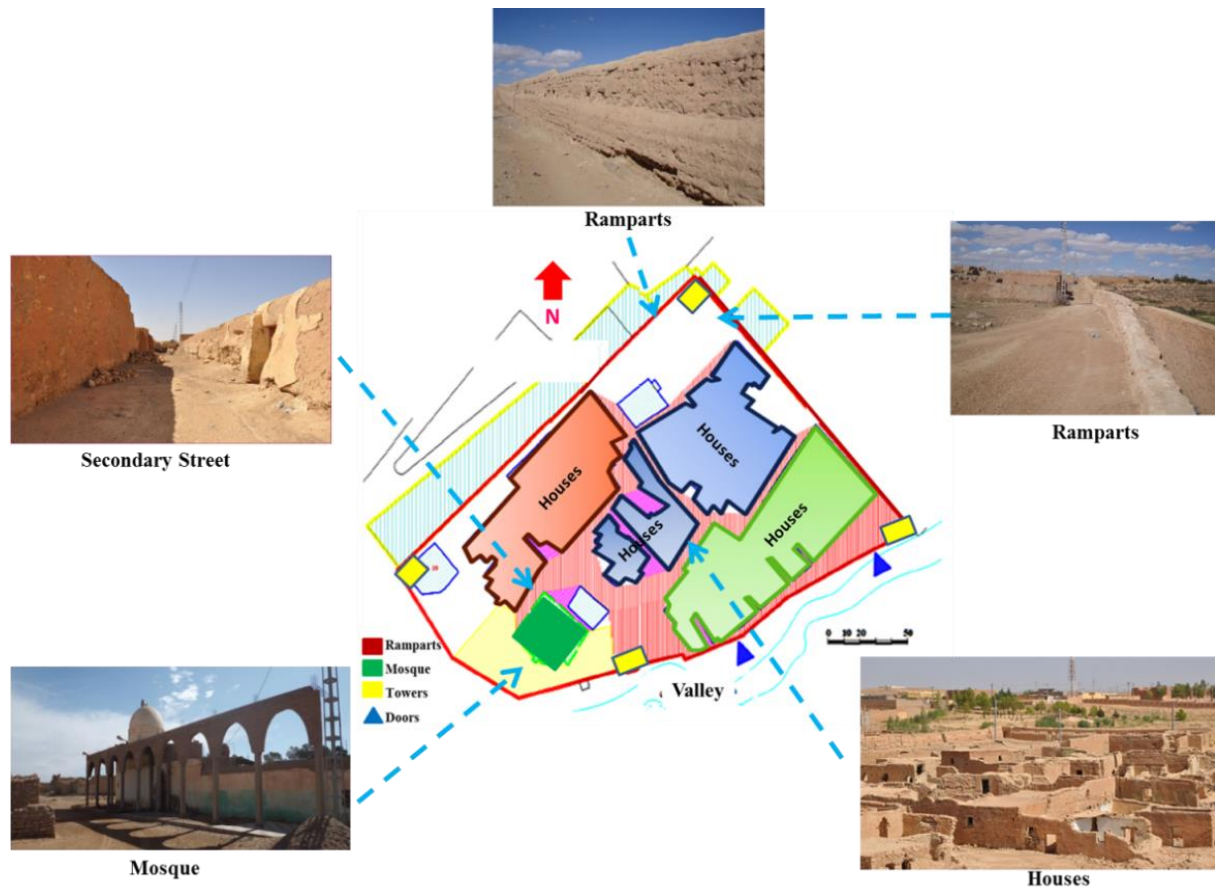


Figure 4. The current state of Ksar Tadjrouna

3.2. Diagnosis

According to several visits to the Ksar, the pathologies noticed in the Ksar Tadjrouna are as follows:

- The use of heterogeneous materials (cement)
- Superficial cracks
- The degradation of the plaster
- Degradation of the base of walls
- The capillary rise
- Degradation of doors.
- Collapse of walls.

Most of the causes of these pathologies are:

- Water stratification
- Absence of maintenance
- Rainwater infiltration.

3.3. The Proposed Strategy (Intervention)

The main objective of our study is the protection of Ksar Tadjrouna through its morphological analysis and the valuation of its tourist potential and the attraction of its inhabitants who have deserted it.

Experience has shown that a comprehensive approach to architectural heritage conservation is imperative for its success. Merely addressing surface-level issues such as filling cracks, renewing plasters, and constructing new buildings may not suffice. A holistic strategy should not only encompass physical restoration but also prioritize community engagement and socio-cultural considerations. Preserving architectural heritage extends beyond the structural aspects; it involves fostering a sense of belonging and identity among the local population.

In instances where conservation efforts are limited to superficial repairs, the result can be a struggle in retaining the current inhabitants. A more nuanced approach that integrates the community into the preservation process is essential. This approach not only ensures the sustainability of the architectural heritage but also enhances the quality of life for the residents.

Furthermore, a one-dimensional focus on physical restoration may not encourage the return of those who have left the area. A successful conservation policy should strive to create an environment that attracts and welcomes back individuals who may have migrated for various reasons. This might involve initiatives that blend modern amenities with historical significance, thereby striking a balance between preservation and contemporary needs.

In essence, a holistic architectural heritage conservation policy should intertwine physical restoration with community involvement, creating a sustainable and vibrant environment that not only preserves the past but also enriches the present and future.

In light of these challenges, we propose a renovation plan which includes various planning operations (rehabilitation and restoration operations), in the objective (i) to provide the Ksar with a basic infrastructure for the inhabitants who still reside there; (ii) and also, to make it find its cultural and spiritual role through the creation of:

- A tourist route inside the ksar which initially passes through the place of the mosque, the typical house (the house of EL-kaid), the place of El-Sahli, the tower.
- Guest houses near the place of EL-Sahli and the restaurant.

These are intended to receive national tourists who come to visit it and attracting international tourists by encouraging cultural tourism. These additions not only cater to national tourists seeking to explore the Ksar but also aim to attract international tourists by promoting cultural tourism, fostering a renewed appreciation for the historical and architectural richness of Ksar Tadjrouna.

4. Conclusions

The Ksar of Tadjrouna has a cultural, historical and tourist importance, it has a particular identity. The nature of urban morphology has been explored as a quantifiable interpretation of the physical form of the Ksar, along with its own theories to explain changes in multiple urban situations.

At the analytical level, we endeavored to conduct a morphological analysis of Ksar Tadjrouna by examining the relationship between space and the successive events that have shaped this Ksar. Additionally, we observed the significance of rehabilitating and

requelifying various systems and components of the Ksar that had undergone degradation and distortion.

This led us to propose recommendations related to specific aspects of urban life and to integrate various dimensions such as social, environmental, and architectural considerations.

- The reassignment of certain heritage buildings to accommodate certain cultural and commercial activities: library, open-air museum restaurant, etc.
- The requalification of public places that have been marginalized.
- Improving the urban landscape through the urban renovation of facades.

All these proposals and solutions were derived from a desirable theoretical framework intended for real-world application. Our ultimate goal is to advocate for the classification of Ksar Tadjrouna as a safeguarded sector, ensuring its conservation as a testament to a rich and characterizing civilization.

Author Statement

The author confirms sole responsibility for the study conception and design, data collection, analysis and interpretation of results, and manuscript preparation.

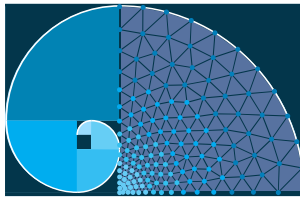
Conflicts of Interest

The author declares that there is no conflict of interest.


References

- Anonymous. (2020). On The World Map, <https://ontheworldmap.com/algeria/>. (Date of access: 03.05.2023)
- Borie, A., & Denieul, F. (1984). Etude et Document sur le Patrimoine Culturel, Méthode d'analyse Morphologique des Tissus Urbains Traditionnels, UNESCO. Paris, France.
- Brik, B., & Smaali, A. (2016). La Réhabilitation Des Ksour De La Veille Ville De Nigrine, Cas D'études: (Types de Maisons Ksouriennes). *Master Thesis*. Larbi Tébéssi-Tébessa University.
- Can, I., & Heath, T. (2016). In-Between Spaces and Social Interaction: A Morphological Analysis of İzmir Using Space Syntax. *Journal of Housing and the Built Environment*, 31, 31-49.
- Cömert, N. Z. (2013). Testing an Integrated Methodology for Urban Typo-morphological Analysis on Famagusta and Ludlow (Publication No. 11129/656). *Doctoral Dissertation, Eastern Mediterranean University*. Eastern Mediterranean University Institutional Repository.
- Direction De La Culture De Laghouat. (2017). «Etude Des 5 Ksours De Laghouat ».
- Dłużewska, A., & Dłużewski, M. (2017). Tourism Versus The Transformation of Ksours-Southern Morocco Case Study. *Bulletin of Geography. Socio-economic Series*, (36), 77-86.
- Goodarzi, P., Ansari, M., Mahdavinejad, M., Russo, A., Haghighatbin, M., & Rahimian, F. P. (2023). Morphological Analysis of Historical Landscapes Based on Cultural DNA Approach. *Digital Applications in Archaeology and Cultural Heritage*, 30, e00277.

- Hamma W. (2011). Intervention Sur LePatrimoine Urbain, Acteurs Et Outils, Le Cas De La Ville Historique De Tlemcen (Publication No. 112/10733). *Master Thesis*. Abou Bekr Belkaid Tlemcen University.
- Kristjánsdóttir, S. (2019). Roots of Urban Morphology. *ICONARP International Journal of Architecture and Planning*, 7, 15-36.
- Li, Z., & Hu, D. (2022). Exploring The Relationship Between The 2D/3D Architectural Morphology and Urban Land Surface Temperature Based on a Boosted Regression Tree: A Case Study of Beijing, China. *Sustainable Cities and Society*, 78, 103392.
- Mazouz. F. (2015). Le Renouveau Du Patrimoine Bâti Vétuste -Le Cas Du Centre-Ville d'Oran. *Doctoral Dissertation, University of Science and Technology of Oran Mohamed-Boudiaf*.
- PPMVSA. (2018). Plan Permanent de Mise en Valeur et de Sauvegarde des Sites Archéologiques, la direction de la culture de la wilaya de Laghouat. "Permanent Plan for the Development and Protection of Archaeological Sites, cultural department of Laghouat". Project leader: Chettih Azzedine, Studies Office: Sahli Faisal.
- Prokopska, A. (2001). Application of Morphological Analysis Methodology in Architectural Design. *Acta Polytechnica*, 41(1), 46-54.
- Scheer, B. C. (2017). Urban Morphology as a Research Method. *Planning Knowledge and Research*, 167-181.
- The Burra Charter. (2013). The Australia ICOMOS Charter for Places of Cultural Significance.
- Topçu, M., & Kubat, A. S. (2012). Old and New City: Morphological Analysis of Antakya. In *8th International Space Syntax Symposium* (pp. 1-16).
- UNESCO. (2003). UNESCO Convention for the "Safeguarding of the Intangible Cultural Heritage".
- UNESCO. (2019). Operational Guidelines for the Implementation of the World Heritage Convention. United Nations Educational, Scientific and Cultural Organization, Intergovernmental Committee for the Protection of the World Cultural and Natural Heritage.
- Wang, X., Song, Y., & Tang, P. (2020). Generative Urban Design Using Shape Grammar and Block Morphological Analysis. *Frontiers of Architectural Research*, 9(4), 914-924.



Application of Inelastic Nonlinear Buckling Analysis with Stiffness Reduction Factors to Web Tapered I Sections

Oğuzhan Toğay* 

¹ Izmir Kâtip Çelebi University, Faculty of Engineering and Architecture, Department of Civil Engineering, İzmir, Türkiye

* Corresponding author: oguzhan.togay@ikcu.edu.tr

Received: 5.01.2024

Accepted: 29.01.2024

Abstract

This paper explores the application of Inelastic Nonlinear Buckling Analysis (INBA) with Stiffness Reduction Factors (SRFs) in the analysis of web-tapered I sections, a structural configuration known for its non-uniform geometry. Leveraging the advanced capabilities of the SABRE2-V2 software, the study investigates the direct load capacity of members and frames, focusing on the implications for structural efficiency and steel material utilization. The inclusion of fixed brace conditions at the midpoint of the beam member, with non-uniform bending, expands the applicability of INBA to complex configurations. The research validates the analytical methods through comparison with Finite Element Analysis (FEA) with four cases that includes different taper angle, achieving an average 98.6% consistency. The study unveils a characteristic S-shaped buckling pattern influenced by strategically placed braces, providing valuable insights into stability and performance optimization. Furthermore, INBA coupled with SRFs elucidates yielding patterns within the member, contributing to a comprehensive understanding of load-carrying behavior and potential failure mechanisms. The findings support the broader adoption of INBA for web-tapered I sections, offering engineers reliable tools for enhanced structural analysis and design. The paper concludes with implications for future research, suggesting exploration of varied taper angles, loading conditions, and material properties.

Keywords: Web-tapered I sections, Inelastic Nonlinear Buckling Analysis (INBA), Stiffness Reduction Factors (SRFs), structural efficiency

1. Introduction

The evolution of structural engineering methodologies has spurred innovative approaches to enhance the analysis and design of steel structures, particularly those with complex geometries. This paper delves into the application of Inelastic Nonlinear Buckling Analysis (INBA) with Stiffness Reduction Factors (SRFs) in the analysis of web tapered I sections – a structural configuration recognized for its non-uniform geometry. The exploration of INBA with SRFs is facilitated through the advanced capabilities of the SABRE2-V2 software, developed by White et al. (2022), offering valuable insights into the direct load capacity of members and frames.

The consideration of web-tapered members holds paramount importance, not only in terms of structural performance but also in terms of the efficient utilization of steel material, positively

impacting economic aspects. Optimizing the use of steel material becomes crucial for achieving structural efficiency, and this paper aims to contribute insights into optimizing the design of web tapered I-sections.

In this topic, Yang and Yau (1987) studied the stability of I beams with tapered webs using differential equations. Andrade et al. (2005) and Boissonnade and Maquoi (2005) showed that prismatic beam elements can be used for the analysis of tapered beams, but without taking into account the bracing strength requirements. Marques et al. (2012), Marques et al. (2013) and Marques et al. (2014) proposed new methods for assessing the resistance of web-tapered columns, beams and beam-columns, based on the Eurocode principles for stability design of members. Recently, Asgarian et al. (2021) presented a theoretical and numerical model based on the power series method for the lateral buckling stability of tapered thin-walled beams with arbitrary cross-sections and boundary conditions. Design Guide 25 (White et al., 2021) provided guidance for the design of web tapered members using different types of braces at various locations and verified the member resistances with hand calculations.

In this study, a distinctive focus is placed on the implementation of fixed brace conditions at the midpoint of the beam member using non-uniform bending. This configuration results in zero moment at one support, gradually increasing linearly towards the other. The utilization of fixed brace conditions introduces a novel dimension to the analysis, broadening the applicability of INBA beyond single-opening members to more complex configurations. This inclusion of bracing applications becomes particularly significant as it expands the scope of INBA, making it applicable not only to conventional members but also to those with intricate geometries and varying support conditions.

While SABRE2-V2, by design, provides direct load capacity information, this study acknowledges the software's limitation in providing detailed post-buckling information. Nonetheless, the software's capacity to simulate inelastic behavior lays the groundwork for a comprehensive exploration of buckling phenomena and initial responses in steel structures.

The literature has highlighted the importance of accurate and reliable analysis methods for predicting the behavior of steel structures with non-uniform geometries. Design Guide (DG25), a document offering suggested methods for the design of web-tapered I-shaped beams and columns, as well as frames incorporating such elements, plays a pivotal role in shaping industry standards. Historical studies by Butler and Anderson (1963) and Prawel et al. (1974) contribute to the understanding of the elastic stability of web and flange tapered beams. Butler and Anderson (1963) focused on investigating the prerequisites for bracing, while Prawel et al. (1974) delved into the topic of inelastic stability, notably considering fixed braces in their experimental analyses.

Building upon this historical and contemporary foundation, White et. al. (2022)'s pioneering work in the development of SABRE2-V2 and its application to INBA with SRFs positions this research at the forefront of advancing the capabilities of structural analysis tools.

As the subsequent sections unfold, this paper will present a detailed theoretical framework of INBA, focusing on the unique application of fixed brace conditions for web tapered I sections. By systematically exploring the effectiveness of this method, considering the non-uniform nature of web tapered I-sections, the research seeks not only to address existing gaps in the literature but also to provide practical insights that can inform the design and assessment of steel structures with enhanced efficiency and structural integrity.

2. Methodology

2.1. Modeling Tapered I Sections with Varying Taper Angles

The paper focuses on assessing the correctness and reliability of the Inelastic Nonlinear Buckling Analysis (INBA) method by investigating the influence of taper angle (α) on the structural behavior of web tapered I sections. Four different values of α —namely, 3, 3.2, 3.4, and 3.6—are considered for the analysis (Figure 1). The modeling of these tapered sections is conducted using two distinct software platforms: ABAQUS Finite Element Software (Simulia, 2020) and SABRE2 (White et. al., 2022).

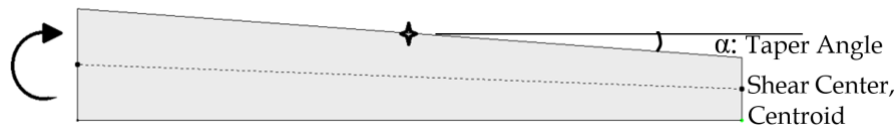


Figure 1. Test figure of I-tapered web steel sections

2.1.2. Finite Element Analysis (FEA)

The initial aspect of the analysis involves utilizing ABAQUS (Simulia, 2020) to simulate the structural response of the web tapered I sections. The FEA is conducted employing an inelastic nonlinear buckling analysis methodology. The analysis takes into account both residual stresses and geometric imperfections to critically evaluate the correctness of the INBA method under varying taper angles.

2.1.2.1. Residual Stress

The analysis in this study leverages the Best-fit Prawel pattern (Figure 2) within its shell finite element models (FEA) to accurately account for residual stresses. This specific pattern, lauded for its self-equilibrating nature within individual components, has proven effective in past research conducted by Kim (2010) and Subramanian and White (2017). While an alternative approach utilizing half the Best-fit Prawel pattern was considered as suggested from Kim (2010), the full pattern demonstrably exhibited a closer alignment with real-world case studies documented by Smith et al. (2013). Notably, this improved correspondence reinforces the suitability of the Best-fit Prawel pattern (Figure 3) for capturing the intricate residual stress distributions typically encountered in metal building members, as previously investigated by Smith et al. (2013). The preference for the full pattern over the half-pattern further underscores its efficacy in replicating the actual behavior observed in practical engineering scenarios.

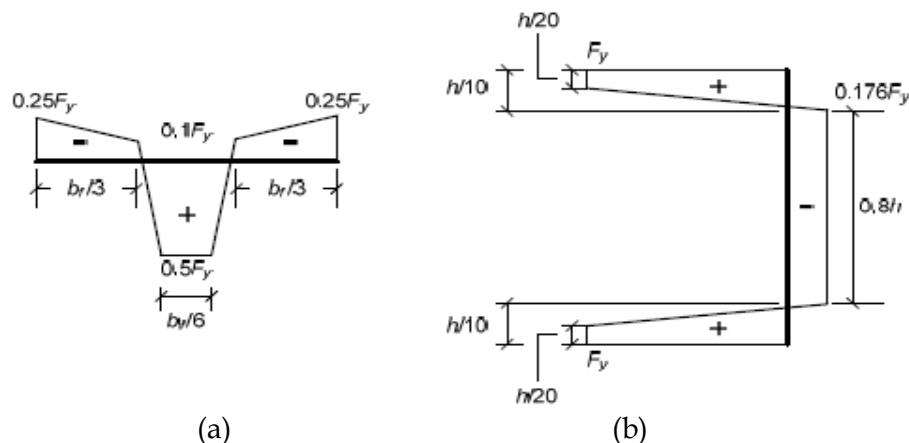


Figure 2. Best-fit Prawel Pattern (a) flange distribution, (b) web distribution
(Adapted from Lokhande, 2014)

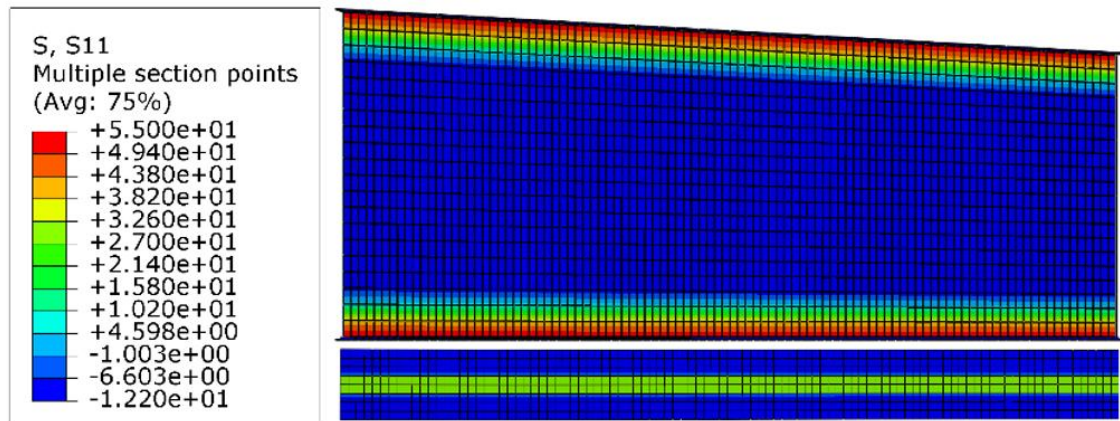


Figure 3. Applied Best-fit Prawel Pattern on $\alpha=3.2$ case ($L_b=127$ cm)

2.1.2.2. Geometric Imperfections

To model realistic geometric imperfections in the test simulations, the study adopts half of the tolerance values from the AWS (2010)/AISC Code of Standard Practice (COSP) (2022). This choice is presented by Subramanian and White (2017) demonstrating a strong correlation between these imperfections and experimental data.

To precisely capture web out-of-flatness and flange tilt patterns, the study employs an elastic eigenvalue buckling analysis. This involves subjecting the members to uniform axial compression while strategically restraining out-of-plane displacements at the web-flange juncture points. The resulting buckling modes inform the fine-tuning of flange tilt and web out-of-flatness patterns, ensuring they conform to the specified tolerance values (see Figure 4).

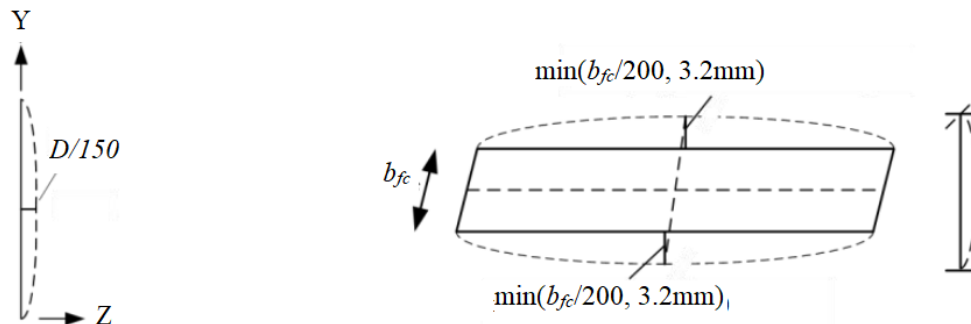


Figure 4. One half of the web out-of-flatness and flange tilt imperfection, adapted from Toğay and White (2017) using Subramanian and White (2017)

Beyond the initial geometric imperfections, the study further complicates the Critical Segment (CS) by introducing a flange sweep at the weld junctions between web and flanges. This sweep, resembling a subtle sinusoidal wave, ripples across the upper flange, which experiences bending under compression. However, the lower flange, subjected to opposite bending forces of tension, remains resolutely straight, devoid of any sweep. This nuanced approach to flange imperfections, captured in Figure 5, adds another layer of complexity to the model, potentially reflecting real-world behavior or serving a specific analytical purpose. The precise details of the sweep's amplitude or wavelength, if relevant, would further illuminate its significance in the study's overall findings.

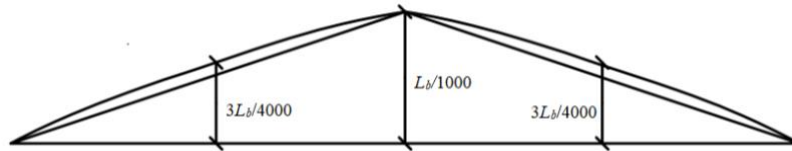


Figure 5. Applied half of the imperfections (the AWS/ AISC COSP flange sweep tolerance) on the critical unbraced length, adapted from Toğay and White (2017) using Subramanian and White (2017)

An example model using the above geometric imperfections is presented in Figure 6. The presented figure has $\alpha=3.2$ and scale factor of 200.

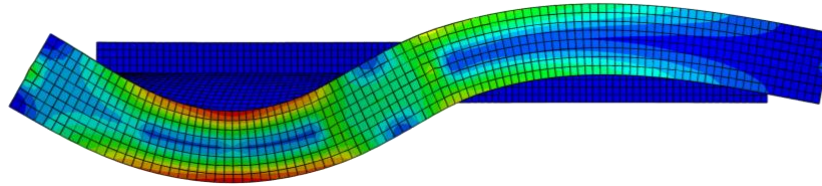


Figure 6. Applied half of imperfections to the finite element model for $\alpha=3.2$ and scale factor=200 with the S11 stresses plotted

2.1.3. Material Properties

This study utilizes a specific stress-strain curve (Figure 7) to define the steel properties in all test models. The beams are modeled as homogenous materials with a yield strength (F_y) of 379.211 MPa and an elastic modulus (E) of 200 GPa. They behave elastically until reaching a strain of ϵ_y , followed by a slight increase in hardness until a strain-hardening point at 10 times the yield strain ($10\epsilon_y$).

Based on the assumed yield strength and the minimum ultimate strength for A572 Grade 55 steel reported by Kim (2010), an ultimate strength (F_u) of 482.632 MPa is further established. Beyond the strain-hardening point, a constant hardening modulus of $E/50$ is applied, and the material behavior is assumed to be fully plastic, which is not experienced by the members.

It's important to note that the S4R element, which is implemented for the FEA analyses, in ABAQUS software interprets the stress-plastic strain curve logarithmically, which aligns well with the high strains encountered in these simulations. While this approach differs slightly from other true stress-logarithmic strain or engineering stress-strain methods, the discrepancies are minimal. Therefore, the provided stress-strain curve (see Figure 7) offers a reliable approximation of the actual stress-strain behavior of structural steel up to its ultimate strength (F_u).

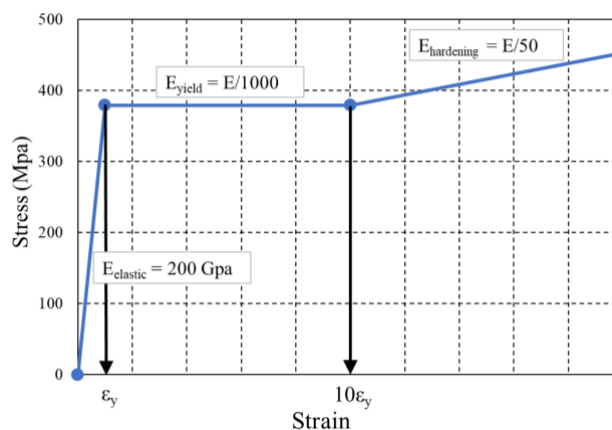


Figure 7. Typical stress-strain curve for $F_y = 55$ ksi (Kim, 2010)

2.2. FEA Model Validation

This study validates its analytical methods by comparing them to a case study presented in Smith et al. (2013). That study examined the lateral buckling behavior of beam-columns under cyclic loading conditions. Since the current study focuses on the inelastic, nonlinear static response, only the first cycle of the experimental data is analyzed.

Among the ten cases presented by Smith et al. (2013), the CF1 case is chosen for validation (Figure 8). This case features a fixed taper angle, constant flange thickness throughout both top and bottom flanges, and a critical segment within the first unbraced length.

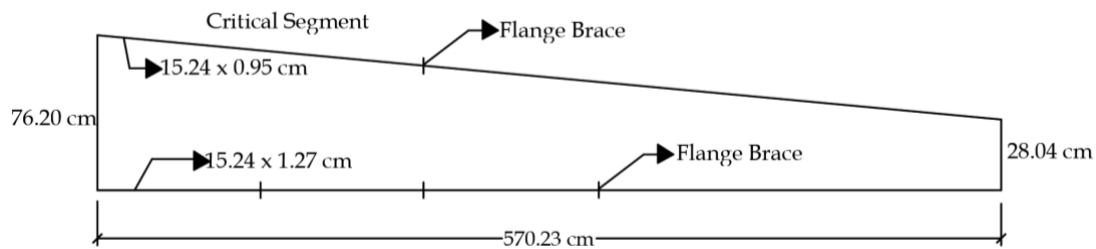


Figure 8. CF1 specimen chosen for the validation study (Smith et. al., 2013)

Figure 9 presents a comparison between the load-deflection curves obtained from the ABAQUS simulations and the actuator load-stiffness data provided by Smith et al. (2013). The values of actuator displacement and force in the simulations are extracted from the support reactions and rotations. From the results of the validation studies, the FEA studies show close correlation with the experimental data.

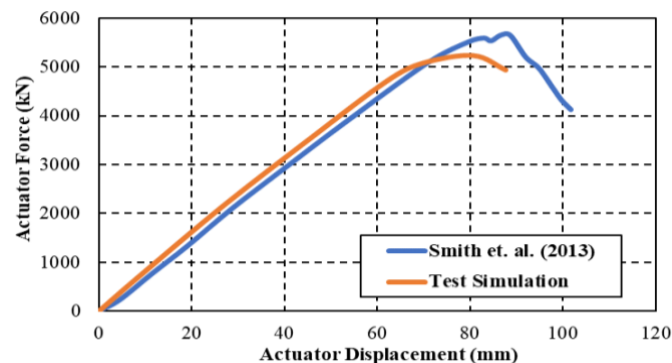


Figure 9. Comparison of test simulations vs the experimental data of Smith et. al. (2013)

2.3. I-Section Steel Members: A Detailed Examination

The section consists of four steel members, each with a length of 254 centimeters and an unbraced length of 127 centimeters. These members exhibit a web depth of 106.68 centimeters on the left side, featuring a constant thickness of 1.463 centimeters. The taper angles (α) at the top flange location vary from 3 to 3.6 degrees, progressing from the start to the end. The top and bottom flanges maintain a consistent flange width of 22.86 centimeters and a flange thickness of 1.905 centimeters.

The members are supported at both ends, with a fixed top point brace located at the midpoint. The material properties include a yield strength (F_y) of 378.5 MPa for both the web and the top and bottom flanges. The structural model utilizes SABRE2-v2 (White et. al., 2022), as illustrated in Figure 10.

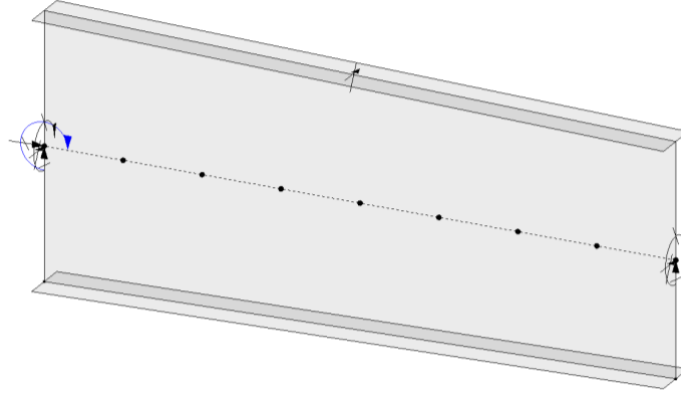


Figure 10. An example model of taper angle 3.0 using SABRE2-V2 (White et. al., 2022)

3. Inelastic Nonlinear Buckling Analysis using Stiffness Reduction Factors

In this section, the stiffness reduction factors (SRFs) for axial, bending, and combined axial and bending loads are given. To keep the paper succinct, only the related equations are given. The derivations of these equations can be found in Toğay (2018).

- Column inelastic stiffness reduction factor, τ_a , is given in Eq. (1) and Eq. (2).

- For $\left(\frac{\Gamma P_u}{\phi_c P_y} > 0.390 \right)$ inelastic buckling controls,

$$\tau_a = -2.724 \frac{\phi_c P_n}{\phi_c P_y} \ln \left(\frac{\phi_c P_n}{\phi_c P_y} \right) \quad (1)$$

- For $\left(\frac{\Gamma P_u}{\phi_c P_y} \leq 0.390 \right)$ elastic buckling controls,

$$\tau_a = 1 \quad (2)$$

where: $\phi_c P_n$: the column factored resistance,

ΓP_u : internal axial force,

$\phi_c P_y$: the column factored axial yield strength,

- Beam inelastic stiffness reduction factor, τ_{ltb} , when compact and noncompact web I-section members with $m > \frac{F_L}{F_{yc}}$, where $\phi_b M_{max.LTB} = 0.9 R_b R_{pc} M_{yc}$, is given in Eq. (3).

$$\tau_{ltb} = \sqrt{\frac{Y^4 X^2}{6.76 X^2 \left(\frac{F_{yc}}{E} \right)^2 m^2 + 2Y^2}} \quad (3)$$

where: X and Y are given in Eq. (4) and Eq. (5), respectively.

$$Y = m \left[\frac{\left(1 - \frac{m}{R_{pc}}\right) \left(\frac{L_r}{r_t} - \frac{L_p}{r_t}\right) + \frac{L_p}{r_t} \left(\frac{F_{yc}}{E}\right) \left(\frac{1}{1.95}\right)}{\left(1 - \frac{F_L}{R_{pc} F_{yc}}\right)} \right] \quad (4)$$

$$X^2 = \frac{S_{xc} h_o}{J} \quad (5)$$

- for slender-web I-sections τ_{ltb} is given in Eq. (6).

$$\tau_{ltb} = \frac{m}{R_b} \left[\frac{\left(R_h - m \frac{1}{R_b}\right) \left(\sqrt{\frac{F_{yc}}{F_L}} - \frac{c}{\pi}\right) + \frac{c}{\pi}}{\left(R_h - \frac{F_L}{F_{yc}}\right)} \right]^2 \quad (6)$$

where: c is 1.1 for the current AISC (2016) Specification and the Stiffness Reduction Factor (SRF) is given in Eq. (7).

$$SRF = 0.9 R_b \tau_{ltb}. \quad (7)$$

4. Results and Discussion

To validate the INBA results presented in Section 2.3, the same members were analyzed using two different software packages: SABRE2-v2 and ABAQUS. SABRE2-v2 utilized an Inelastic Nonlinear Buckling (INBA) approach with Stiffness Reduction Factors (SRFs), while ABAQUS employed Inelastic Nonlinear finite element analysis.

Figure 11 compares the results obtained from both methods, showing the percentage difference between INBA and Finite Element Analysis (FEA) solutions. Notably, the average difference between the two approaches is a mere 1.4%, demonstrating a average 98.6% consistency. This agreement provides strong confidence in the reliability of the INBA results presented earlier.

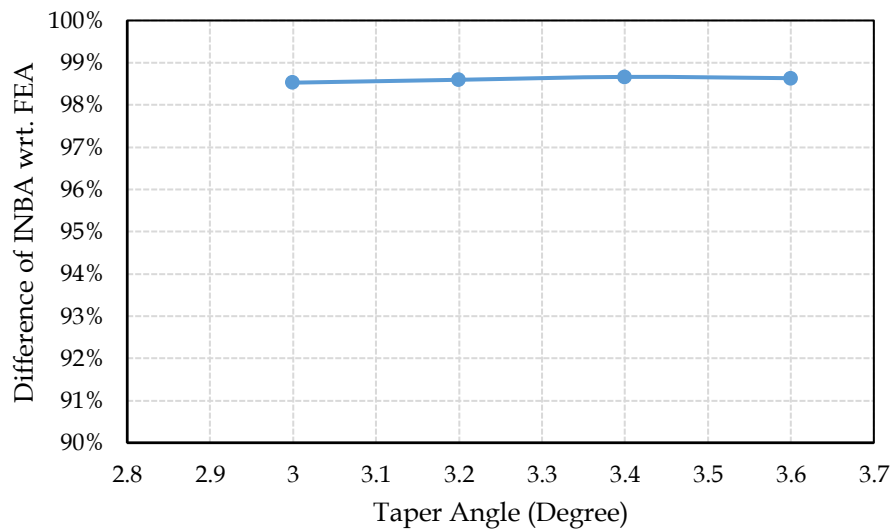


Figure 11. Percentage difference of Inelastic Nonlinear Buckling Analysis (INBA) vs FEA simulations

Figure 12 illustrates the characteristic S-shaped buckled form of a 3.0 taper angle member. Significantly, both the Inelastic Nonlinear Buckling Analysis (INBA) and Finite Element Analysis (FEA) methods yield remarkably similar displaced shapes, underscoring the consistency observed in the quantitative results. This agreement reinforces the validity of the INBA approach for predicting buckling behavior in tapered angle members.

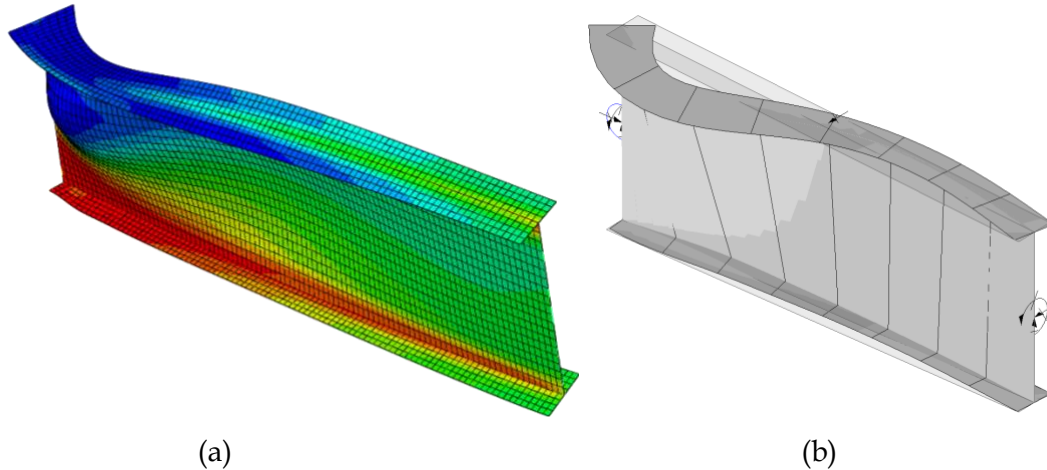


Figure 12. (a) Finite element analysis buckled shape at the peak load incorporating of S11 stresses, (b) SABRE2-V2 buckled shape at the buckling load proportionality factor (LPF)

The S-shaped buckling pattern is primarily governed by the strategic placement of the brace. By effectively restricting out-of-plane displacement, the brace compels the member to buckle within its own plane, resulting in the distinctive S-shaped configuration.

Beyond predicting buckling behavior, Inelastic Nonlinear Buckling Analysis (INBA) unveils crucial insights into yielding patterns through Stiffness Reduction Factors (SRFs). These factors quantify the extent of yielding within structural sections, acting as indispensable indicators of a member's overall capacity to resist deformation.

The SRF plot generated for the tapered angle member in SABRE2-v2 paints a vivid portrait of yielding distribution (Figure 13). It reveals a striking gradient of SRF values, commencing at a minimum of 0.147 on the left side and culminating in a maximum of 1.0 on the right side. This gradient conveys several key interpretations:

- **Yielding Localization:** The low SRF value of 0.147 on the left side signals substantial yielding within that region, indicating a concentration of plastic deformation. This localization likely stems from a combination of factors, including geometric variations, stress concentrations, or material inhomogeneities.

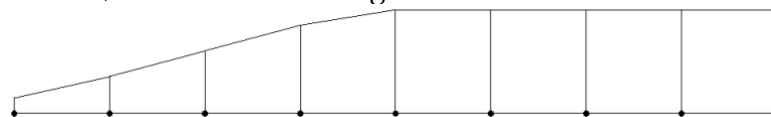


Figure 13. SRF plot of taper angle of 3.0

- **Unyielded Region:** Conversely, the SRF value of 1.0 on the right side signifies a complete absence of yielding, implying the material in that region remains within its elastic range. This disparity in yielding patterns highlights the complex interplay between member geometry, loading conditions, and material properties.
- **Yield Progression:** The gradual increase in SRF values from left to right suggests a progressive transition from a highly yielded state to an unyielded state along the member's length. This pattern offers valuable insights into the member's load-carrying behavior and potential failure mechanisms. The PEEQ contour of the member with a

taper angle of 3.0 exhibits a close correlation with the SRF plot (Figure 14). Non-zero PEEQ values are colored red, indicating the spread of yielding at the peak load proportional factor, while zero PEEQ values are blue, illustrating where the plates remain elastic. This observation enhances the understanding of the specific behavior of the tapered member under load, providing a comprehensive view of its structural response and failure characteristics.

- Safety Factor Considerations: While a safety factor of 0.9 is typically applied in design practice to account for uncertainties, its omission in this analysis facilitates a direct comparison with Finite Element Analysis (FEA) results, ensuring a consistent basis for validation.

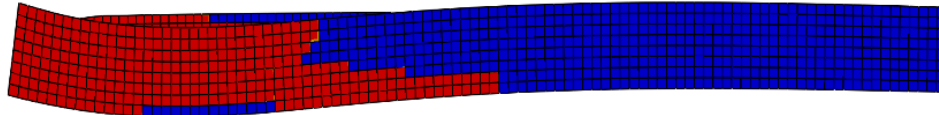


Figure 14. PEEQ contours on the deformed geometry from the top view (scale factor: 1)

5. Conclusions

This research has systematically investigated the application of Inelastic Nonlinear Buckling Analysis (INBA) with Stiffness Reduction Factors (SRFs) to web tapered I sections, a growing trend in modern steel design. The findings provide valuable insights into the buckling behavior of these complex elements, paving the way for optimized design and analysis techniques.

The significant agreement between INBA and Finite Element Analysis (FEA) results, with a remarkable 98.6% consistency, validates the accuracy and robustness of INBA for assessing the buckling response of web tapered I sections, particularly those with fixed brace configurations. This validation paves the way for the broader adoption of INBA in this domain, enhancing the reliability and efficiency of structural analysis for these increasingly popular elements.

Furthermore, the analysis revealed the characteristic S-shaped buckling pattern observed in the test member, a direct consequence of the strategically placed fixed brace. This observation highlights the effectiveness of the brace in mitigating out-of-plane deformations, offering valuable guidance for engineers seeking to optimize the stability and performance of web tapered I sections in their designs.

Beyond predicting buckling behavior, INBA coupled with SRFs provides crucial insights into the internal distribution of yielding within the member. The gradient of SRF values, indicative of concentrated plastic deformation on one side and an unyielded region on the other, illuminates the member's load-carrying capacity and potential failure mechanisms. This knowledge empowers engineers to design more robust and resilient structures, maximizing the efficiency and lifespan of web tapered I sections.

While this research has made significant strides in understanding the nuances of web-tapered I sections, it also acknowledges the need for further investigation. Future research could explore the influence of various taper angles, loading conditions, and material properties on their buckling behavior and yielding patterns. Additionally, analyzing the response of these elements under dynamic or cyclic loading could offer valuable insights for practical applications.

Author Statement

The author confirms sole responsibility for the following: study conception and design, data collection, analysis and interpretation of results, and manuscript preparation.

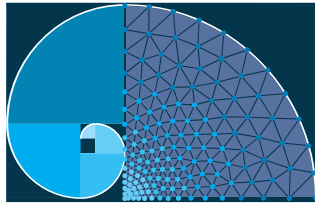
Conflict of Interest

The authors declare no conflict of interest.


References

- AISC (2016). Specification for Structural Steel Building. *American Institute of Steel Construction*.
- AISC (2022). Specification for Structural Steel Building. *American Institute of Steel Construction*.
- AWS (2010). Structural Welding Code–Steel, AWS D1.1: D1.1M, (22nd ed.), prepared by AWS Committee on Structural Welding, 572.
- Andrade, A., Camotim, D., & e Costa, P.P. (2005). Elastic Lateral-Torsional Buckling Behavior of Doubly Symmetric Tapered Beam-Columns Proceedings. *Annual Stability Conference, Structural Stability Research Council, Montreal, Quebec, Canada*, 445-468
- Asgarian, B., Soltani, M., & Mohri, F. (2013). Lateral-torsional Buckling of Tapered Thin-Walled Beams with Arbitrary Cross-sections. *Thin-Walled Structures*, 62, 96-108,
- Boissonnade, N., & Maquoi, R. (2005). A Geometrically and Materially Non-linear 3-D Beam Finite Element for the Analysis of Tapered Steel Members, *Steel Structures*, 5, 413-419.
- Butler, D. J., & Anderson G. C. (1963). The Elastic Buckling of Tapered Beam-Columns. *Welding Journal Research Supplement*.
- Kim, Y. D. (2010). Behavior and Design of Metal Building Frames with General Prismatic and Web-Tapered Steel I-Section Members. *Doctoral Dissertation*. School of Civil and Environmental Engineering, Georgia Institute of Technology, Atlanta, GA, 562 pp. n.d.
- Lokhande, A. M. (2014). Evaluation Of Steel I-Section Beam And Beam-Column Bracing Requirements By Test Simulation, *Master Thesis*, School of Civil and Environmental Engineering, Georgia Institute of Technology, Atlanta, GA.
- Marques, L., Taras, A., Simões da Silva, L., Greiner, R., & Rebelo, C. (2012). Development of a Consistent Buckling Design Procedure for Tapered Columns. *Journal of Constructional Steel Research*, 72, 61-74.
- Marques, L., Simões da Silva, L., Greiner, R., Rebelo, C. and Taras, A. (2013). Development of a Consistent Design Procedure for Lateral-Torsional Buckling of Tapered Beams. *Journal of Constructional Steel Research*, 89, 213-235.
- Marques, L., Simões da Silva, L., Rebelo, C., & Santiago, A. (2014). *Extension of EC3-1-1 Interaction Formulae for the Stability Verification of Tapered Beam-Columns*, 100, 122-135
- Prawel, S. P., Morrell M. L., & Lee G. C. (1974). Bending and Buckling Strength of Tapered Structural Members, *Welding Research Supplement*, 53, 75-84.
- Simulia. (2020). ABAQUS , Version 6.20. *Software and Analysis User's Manual*.
- Smith, M. D., Turner, K. A., & Uang, C. M. (2013). Experimental Study of Cyclic Lateral-Torsional Buckling of Web-Tapered I-Beams. Report No. SSRP-12/06, *Final Report to Metal Building Manufacturers Association*, Department of Structural Engineering, Univ.

- Subramanian, L., & White, D. W. (2017). Resolving the Disconnect between Lateral Torsional Buckling Experimental Tests, Test Simulations and Design Strength Equations. *Journal of Constructional Steel Research*, 128, 321-334.
- Toğay, O. (2018). Advanced Design Evaluation Of Planar Steel Frames Composed Of General Nonprismatic I-Section Members. *Doctoral Dissertation*, School of Civil and Environmental Engineering, Georgia Institute of Technology, Atlanta, GA, 273 pp.
- Toğay, O., & White, D. W. (2017). Comprehensive Stability Design of Steel Members and Systems via Inelastic Buckling Analysis–Beam-Column Validation Studies. *Proceedings of the Annual Stability Conference Structural Stability Research Council*. San An.
- White, D. W., Jeong, W. Y. & Slein, R. (2021). Frame Design Using Nonprismatic Members, *AISC/MBMA Design Guide 25*, 2nd Ed., American Institute of Steel Construction, Chicago, IL, 405
- White, D. W., Toğay, O. W., Jeong, Y., & Slein, R. (2022). *SABRE2-V2*. white.ce.gatech.edu/sabre.
- Yang, Y. B., & Yau, J. D. (1987). Stability of Beams with Tapered I-Sections. *ASCE J. Eng. Mech.*, 113 (9), 1337–1357.



Innovative Approaches to Modeling Economic Dynamics: Taylor Matrix Methods in Solving Budget Constraint Differential Equations

Nurcan Baykuş Savaşaneril* 

Dokuz Eylül University, Vocational School, İzmir, Türkiye

* Corresponding author: nurcan.savasaneril@deu.edu.tr

Received: 22.12.2023

Accepted: 21.01.2024

Abstract

In recent times, the consensus has emerged that a profound understanding of mathematics is essential to excel as an economist, leading to a rapid increase in the number of articles incorporating mathematical methodologies within the field of economics. This study explores the dynamic aspects of economic modeling by focusing on the budget constraint equation of a group, treating it as a partial differential equation. The budget constraint problem is a common economic challenge where individuals or entities face limitations on consumption choices due to financial constraints. We introduce an alternative method for solving this equation, employing a matrix-based approach grounded in collocation points and Taylor polynomials. This technique streamlines the resolution process, transforming the solution of the group's budget constraint differential equation into a system of matrix equations featuring unknown Taylor coefficients. The paper contributes to the ongoing discourse on mathematical models in economics by presenting an innovative methodology that enhances economists' analytical toolkit for understanding and navigating the intricate dynamics of economic systems. The proposed method is then applied to the budget constraint equation of the group, providing a systematic and efficient approach to obtain numerical solutions. The study includes a numerical example to illustrate the application of the technique, demonstrating its efficiency, precision, and ability to yield highly accurate approximations for the budget constraint equation. The results highlight the versatility and effectiveness of the Taylor matrix-collocation techniques in solving economic problems.

Keywords: Mathematical economics, economics-mathematics relationship, group's budget constraint differential equation

1. Introduction

In the contemporary view of economic research, the interdependent relationship between mathematics and economics has become increasingly evident. A deep understanding of mathematical principles is widely recognized as crucial for achieving excellence in the field of economics, necessitating further exploration and integration of mathematical methodologies through ongoing research. Among the diverse mathematical tools at economists' disposal, differential equations have emerged as powerful instruments for modeling and analyzing various

complex systems. Traditionally associated with physical and engineering problems, these equations have found substantial applications in economics, risk theory, and various social sciences. Differential equations, especially partial differential equations (PDEs), serve as powerful tools for modeling, analyzing, and addressing a wide range of physical and engineering problems. As a crucial branch of applied mathematics, they find application in diverse fields such as network design, fluid dynamics, wave motion, telecommunications, electromagnetic wave distribution, and electronic dynamics. Beyond engineering and physical systems, these equations play a pivotal role in economics, risk theory, and numerous social sciences. In recent years, the development of numerical methods has provided effective solutions for solving these equations. On the other hand, some researchers have criticized the use of mathematical models in the relationship between mathematics and economics. Beed and Kane (1991) provided an overview of the varied and scattered criticisms directed at the mathematization of economics over the last seventy years, highlighting limited comprehensive reviews of the arguments against the emphasis on mathematics in contemporary economics. Bilgin (2006) critically examined the role of mathematical methods in economics, weighing arguments that emphasize the clarity and precision of mathematical approaches against concerns about the potential for unfruitful outcomes in economic theory due to over-reliance on math without a solid theoretical foundation. Aydın (2016) suggested that the relationship between economics and mathematics, particularly within the context of neoclassical economic theory, has been a subject of criticism. Kaleci and Buluş (2016) explored the historical context of the integration of mathematics into economics, examining both positive and negative criticisms, highlighting the current significance of mathematics in economics, and investigating its specific applications within the field. Yücel (2022) advocated that an overdependence on mathematical models, leading to a detachment of economics from social realities, signifies a precarious and perilous situation.

In literature, many researchers have explored diverse aspects of mathematical modeling in economics, ranging from continuous-time heterogeneous agent models and PDE-based approaches in socio-economic processes to the impact of knowledge on wealth evolution and challenges associated with optimal control problems in economic growth theory. Achdou et al. (2014) reviewed the literature on continuous-time versions of heterogeneous agent models in macroeconomics, emphasizing the common mathematical structure involving coupled nonlinear PDEs, particularly the Hamilton–Jacobi–Bellman equation for optimal control and an equation governing the distribution of individual state variables in the population, known as a mean field game, shedding light on the existing knowledge and identifying avenues for future research. Burger et al. (2014) highlighted the growing significance of PDE-based approaches in modeling socio-economic processes, anticipating that this emerging field will become a focal point in PDE-centered modeling, presenting new mathematical challenges and tools while emphasizing the importance of understanding socio-economic complexity for addressing future challenges. Pareschi and Toscani (2014) introduced and explored a modified nonlinear kinetic equation of Boltzmann type, originally proposed by Cordier et al. (2005), to depict the impact of knowledge on wealth evolution within a system of interacting agents engaged in binary trades. Boucekine et al. (2013) reviewed the application of parabolic PDEs in economic growth theory, highlighting the challenges in solving optimal control problems with infinite time horizons and emphasizing the ill-posedness problem. Brito (2020) reviewed and exemplified the use of differential equations in macroeconomic models.

Our study delves into the realm of economic dynamics by focusing on the budget constraint equation of a group, treating it as a PDE. A budget constraint problem typically arises in

economics and refers to the limitation imposed on an individual or entity's consumption choices by the amount of income or resources available. The fundamental idea is that individuals, households, or firms face constraints on their spending or investment decisions due to their limited financial resources. The budget constraint is often expressed in the form of an equation that represents the relationship between income, prices of goods and services, and the quantity of those goods and services consumed or purchased. Mathematically, it can be represented by an equation which indicates that the total income must be allocated among different goods or services, each with its own price and quantity. The challenge is to optimize the allocation to maximize utility, satisfaction, or profit, subject to the budget constraint. In the context of mathematical modeling, budget constraints are often formulated as optimization problems to find the optimal combination of goods or services that an individual or entity can afford given their budget limitations. Moon and Silver (2000) studied a multi-item newsvendor problem with a budget constraint on replenishment quantities, explicitly considering fixed costs for non-zero replenishments, presenting dynamic programming procedures for cases where demand distributions are assumed known. Vairaktarakis (2000) introduced an alternative approach to stochastic optimization for the multi-item newsboy model with a budget constraint and demand uncertainty, utilizing integer programming models with minimax objectives. Numerous studies (Karabakal et al., 2000; Guo et al., 2017; Şahin et al., 2010; Chekuri and Kumar, 2004) have investigated various aspects of budget constraint problems in the literature.

This paper introduces an alternative method for solving this equation, employing a matrix-based approach grounded in collocation points and Taylor polynomials. The proposed technique streamlines the resolution process, transforming the solution of the group's budget constraint differential equation into a system of matrix equations featuring unknown Taylor coefficients. Then an explanation is presented using Taylor polynomials, providing a new way to approach economic challenges. Through this exploration, the paper contribute to the ongoing discourse on mathematical models in economics, presenting an innovative methodology that enhances the analytical toolkit available to economists for understanding and navigating the intricate dynamics of economic systems.

Many researchers have primarily used Taylor polynomials, along with other types of polynomials, to solve both differential and integral equations. Kurt and Sezer (2008) introduced a practical matrix method for approximating solutions to high-order linear Fredholm integro-differential equations with constant coefficients under initial-boundary conditions, utilizing Taylor polynomials. Kurt and Çevik (2008) proposed a straightforward numerical method for solving the single degree of freedom system using Taylor polynomials in matrix form, allowing for the determination of both particular and general solutions of the differential equation. Biçer and Yalçınbaş (2016) introduced an approximate method using Bernoulli polynomials to solve hyperbolic partial differential equations, demonstrating its validity through matrix transformation, employing a Bernoulli coefficients matrix as the unknown, conducting error analysis based on residual function, and providing illustrative examples for method accuracy. Gümgüm et al. (2018) introduced a numerical matrix-collocation technique utilizing Lucas polynomials and standard/Chebyshev-Lobatto collocation points to address functional integro-differential equations with variable delays and initial conditions, and demonstrated its practicability through illustrative examples. Bayku and Sezer (2017) introduced a collocation method based on hybrid Taylor and Lucas polynomials, for solving a higher-order linear nonhomogeneous pantograph-type delay differential equation with variable coefficients and delays. Erdem Biçer and Yalçınbaş (2019) employed the Bernoulli collocation method to suggest

an approximate solution for the telegraph equation. Elmacı et al. (2022) introduced a matrix-collocation method employing Euler polynomials to approximate solutions for singularly perturbed two-point boundary-value problems, presenting a systematic approach involving algebraic equations, coefficient determination. Çayan et al. (2022) proposed the Laguerre matrix collocation method, based on orthogonal Laguerre polynomials, aiming to decrease computational costs in mathematical models by directly utilizing Laguerre polynomials without transforming them into the truncated Taylor polynomial basis. Savaşaneril (2023) introduced a new and straightforward numerical method for solving the free vibration of a single degree of freedom system using Lucas polynomials in matrix form, allowing for the determination of particular and general solutions. Recently, Çevik and Sezer (2023) provided a brief history of polynomial matrix method, mentioned the types of polynomials utilized in collocation approach, explained its fundamental principles and surveyed engineering applications.

2. The Budget Constraint Equation

In this study, we will explore the budget constraint problem of the group proposed by Brito (2020). Let $w(x, t)$ represent the financial wealth of an individual aged x at time t . Then, the budget constraint equation is given in Eq. (1).

$$\frac{\partial w(x, t)}{\partial t} + \frac{\partial w(x, t)}{\partial x} = s(x, t) + r w(x, t) \quad (1)$$

The general solution of Eq. (1), where $s(x, t)$ is the accumulation of an individual at age x and time t and r is the interest rate, is given in Eq. (2).

$$w(x, t) = \left(\int_0^x s(z, z - x + t) e^{-rz} dz + f(t - x) \right) e^{rx} \quad (2)$$

If the initial (at birth) accumulation is given by $w(0, t) = 0$ and the accumulation function is $s(a, t) = e^{ba(K-a)+gt-c}$, then the solution function is given in Eq. (3).

$$w(a, t) = \frac{\sqrt{\pi}}{2\sqrt{b}} \left(\phi \left(\frac{Kb + g - r}{2\sqrt{b}} \right) - \phi \left(\frac{(K - 2a)b + g - r}{2\sqrt{b}} \right) \right) e^{\frac{K^2 b^2 ((2K+4(t-a))g - 2(K-2a)r)b + (g-r)^2}{4b}} - \frac{c}{r} (1 - e^{ra}). \quad (3)$$

In this study, we introduce a Taylor Collocation Method based on matrix equations (Kurt and Sezer, 2008) for the solution of the equation given in Eq. (1). It is given in Eq. (6).

$$w(x, t) \cong w_N(x, t) = \sum_{m=0}^N \sum_{n=0}^N a_{mn} x^m t^n \quad (4)$$

The objective here is to obtain an approximate solution using this approach, and the unknowns in this solution are represented by the Taylor coefficients denoted as a_{mn} ; $m, n = 1, \dots, N$.

3. Fundamental Relations

To obtain the numerical solution of the group's budget constraint equation using the Taylor Collocation Method, we first compute the unknown function's Taylor coefficients. For this purpose, the solution function of Eq. (1) can be written in matrix form as Eq. (5).

$$w_N(x, t) = \mathbf{X}(x) \bar{\mathbf{X}}(t) \mathbf{A} \quad (5)$$

where $X(x)$, $\bar{X}(t)$, A are presented in Eq. (6), Eq. (7), Eq. (8), respectively.

$$\mathbf{X}(x) = \begin{bmatrix} 1 & x & x^2 & K & x^N \end{bmatrix} \quad (6)$$

$$\bar{\mathbf{X}}(t) = \text{diag}[\mathbf{X}(t) \quad \mathbf{X}(t) \quad \mathbf{X}(t) \quad K \quad \mathbf{X}(t)] \quad (7)$$

$$\mathbf{A} = [\mathbf{A}_0 \quad \mathbf{A}_1 \quad L \quad \mathbf{A}_N]^T, \quad (8)$$

Derivatives of w with respect to x and t are given in Eq. (9) and Eq. (10), respectively.

$$\frac{\partial w}{\partial x} = \mathbf{X}(x) \mathbf{B} \bar{\mathbf{X}}(t) \mathbf{A} \quad (9)$$

$$\frac{\partial w}{\partial t} = \mathbf{X}(x) \bar{\mathbf{X}}(t) \bar{\mathbf{B}} \mathbf{A}, \quad (10)$$

Where B, \bar{B} are presented in Eq. (11), Eq. (12), respectively.

$$\mathbf{B} = \begin{bmatrix} 0 & 1 & 0 & \cdots & 0 \\ 0 & 0 & 2 & \cdots & 0 \\ \vdots & \vdots & \vdots & \ddots & \vdots \\ 0 & 0 & 0 & 0 & N \\ 0 & 0 & 0 & 0 & 0 \end{bmatrix}, \quad (11)$$

$$\bar{\mathbf{B}} = \text{diag}[\mathbf{B}]_{(N+1)^2 \times (N+1)^2} \quad (12)$$

4. Solution Methodology

At this stage of our analysis, we are composed to express the foundational matrix equation corresponding to Eq. (1). This crucial step involves synthesizing the pertinent elements and relationships inherent in our study to construct a comprehensive matrix equation. For this purpose, we express matrix Eq. (5), Eq. (9), and Eq. (10) in relation to Eq. (1), incorporating essential adjustments, resulting in Eq. (13):

$$\mathbf{X}(a) \bar{\mathbf{X}}(t) \bar{\mathbf{B}} \mathbf{A} + \mathbf{X}(a) \mathbf{B} \bar{\mathbf{X}}(t) \mathbf{A} = s(a, t) + r \mathbf{X}(a) \bar{\mathbf{X}}(t) \quad (13)$$

With additional modifications, we reach the following Eq. (14):

$$\mathbf{W} = \{ \mathbf{X}(a) \bar{\mathbf{X}}(t) \bar{\mathbf{B}} \mathbf{A} + \mathbf{X}(a) \mathbf{B} \bar{\mathbf{X}}(t) \mathbf{A} - r \mathbf{X}(a) \bar{\mathbf{X}}(t) \} \quad (14)$$

As a result, we acquire Eq. (15):

$$\mathbf{W}(x, t) \mathbf{A} = \mathbf{G}(x, t). \quad (15)$$

The standard or Chebyshev-Lobatto collocation points used in matrix system are given in Eq. (16), respectively, such that x_i and t_i are the Chebyshev-Lobatto collocation points (Gümgüm et al., 2018) on Ω defined to be:

$$x_i = \frac{a+b}{2} + \frac{a-b}{2} \cos\left(\frac{\pi i}{N}\right), \quad t_j = \frac{c+d}{2} + \frac{c-d}{2} \cos\left(\frac{\pi j}{N}\right) \quad i, j = 0, 1, \dots, N. \quad (16)$$

where $i, j = 0, 1, \dots, N$, $a = x_0 < x_1 < \dots < x_N = b$, $c = t_0 < t_1 < \dots < t_N = d$,

By substituting collocation points into Eq. (14), we can express Eq. (16) as follows in Eq. (17):

$$\mathbf{W}(x_i, t_j) = \left\{ \mathbf{X}(x_i) \bar{\mathbf{X}}(t_j) \bar{\mathbf{B}} - \alpha^2 \mathbf{X}(x_i) \mathbf{B}^2 \bar{\mathbf{X}}(t_j) \right\} \quad (17)$$

At this point, it is possible to formulate the fundamental matrix equation corresponding to Eq. (1) in the following form in Eq. (18):

$$\mathbf{WA} = \mathbf{G} \text{ or } [\mathbf{W}; \mathbf{G}] \quad (18)$$

Here, $W(x_i, t_j)$, A , G are presented in Eq. (19), Eq. (20) and Eq. (21), respectively.

$$\mathbf{W}(x_i, t_j) = [\mathbf{W}_0 \quad \mathbf{W}_1 \quad \mathbf{W}_2 \quad \mathbf{L} \quad \mathbf{W}_N]^T \quad (19)$$

$$\mathbf{A} = [a_{00} \quad a_{01} \quad \mathbf{L} \quad a_{0N} \quad a_{10} \quad \mathbf{L} \quad a_{1N} \quad a_{N0} \quad \mathbf{L} \quad a_{NN}]_{1 \times (+1)^2}^T \quad (20)$$

$$\mathbf{G} = [g(x_0, t_0) \quad g(x_0, t_0) \quad \mathbf{L} \quad g(x_0, t_1) \quad \mathbf{L} \quad g(x_0, t_N) \quad \mathbf{L} \quad g(x_N, t_N)]_{1 \times (+1)^2}^T \quad (21)$$

5. Matrix Representation of Conditions

The initial condition of the Eq. (1) is given as in Eq. (22):

$$\mathbf{W}(0, t) = 0 \quad (22)$$

The matrix form of Eq. (22) can be as follows in Eq. (23):

$$\mathbf{W}(0, t) = \mathbf{X}(0) \bar{\mathbf{X}}(t_i) \mathbf{A} = 0, \quad i = 0, 1, \dots, N \quad (23)$$

Thus, we obtain Eq. (24).

$$\mathbf{UA} = \mathbf{0} \text{ or } [\mathbf{U}; \mathbf{0}] \quad (24)$$

Now, we shall express Eq. (1) in the form of Eq. (3) and then use that form to determine the Taylor coefficients $a_{m,n}; m, n = 1, 2, \dots, N$ for the approximate solution provided in Eq. (19). This is achieved by replacing any row of Eq. (18) with Eq. (24), leading to the creation of the following augmented matrix Eq. (25).

$$[\widetilde{\mathbf{W}}; \widetilde{\mathbf{G}}] = \begin{bmatrix} \mathbf{W} & ; & \mathbf{G} \\ \mathbf{U} & ; & \mathbf{0} \end{bmatrix} \quad (25)$$

The solution to this system of matrix equations provides the Taylor coefficients for the solution function in Eq. (3).

6. Numerical Application

To illustrate the application of the discussed approach, we will now delve into a numerical example addressing the problem given by Brito (2020).

$$K = 88, \quad b = 0.0029, \quad r = 0.02, \quad g = 0.02, \quad c = 50.$$

In accordance with our proposed method for addressing the problem under the specified initial conditions, we utilize collocation points derived from Eq. (16) with $N=5$. Upon computing the approximate solution, the resulting solution function is as follows:

$$\begin{aligned}
 e_{10} = & 894.2290902552949a - 16.92928912951453a^2 + 0.7431029209505327a^3 \\
 & - 0.005142068770569089a^4 + 0.000023867421496233018a^5 - 134.882793421843a^6t + \\
 & + 66.895884054600454a^2t - 0.17570865993074752a^3t + 0.001708040778020449a^4t \\
 & - 6.178284282641527 \cdot 10^{-6}a^5t + 4.3709040726463755a^2t^2 - 0.2662943416850872a^2t^2 \\
 & + 0.006881340967762259a^3t^2 - 0.00007250278180147267a^4t^2 + 2.725177925228526 \cdot 10^{-7}a^5t^2 \\
 & - 0.06564194413920374a^3t^3 + 0.004515561642674559a^2t^3 - 0.00011887445378840342a^3t^3 \\
 & + 1.2916779756873282 \cdot 10^{-6}a^4t^3 - 4.964727260568466 \cdot 10^{-9}a^5t^3 + 0.0004426138874452158a^4t^4 \\
 & - 0.00003309669090596811a^2t^4 + 8.988316952126963 \cdot 10^{-7}a^3t^4 - 1.0041283977949947 \cdot 10^{-8}a^4t^4 \\
 & + 3.945102910652574 \cdot 10^{-11}a^5t^4 - 1.1526531471275705 \cdot 10^{-6}a^2t^5 + 9.200076204012123 \cdot 10^{-8}a^2t^5 \\
 & - 2.5605523746328023 \cdot 10^{-9}a^3t^5 + 2.915848456262097 \cdot 10^{-11}a^4t^5 - 1.1639536893915662 \cdot 10^{-13}a^5t^5
 \end{aligned}$$

Figure 1 illustrates the above numerical result obtained through the proposed technique.

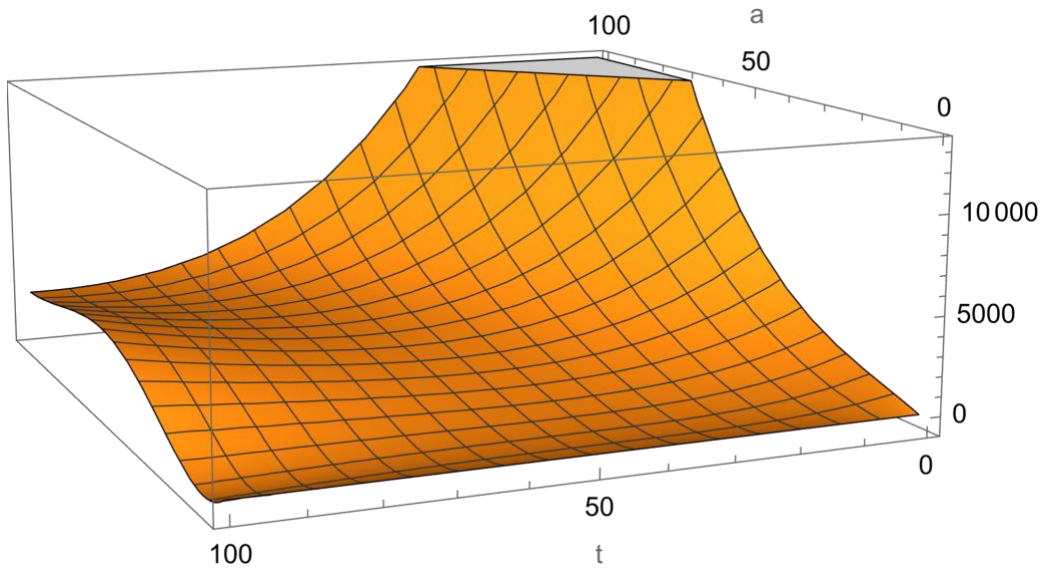


Figure 1. The illustration of the numerical result for the budget constraint differential equation. As can be understood from the results, the individual tends to be a clear debtor in young age and a creditor in old age.

7. Conclusions

We have introduced a novel approach utilizing Taylor matrix-collocation techniques to address the budget constraint equation of the group. This methodology facilitates the seamless transformation of the group's budget constraint equation, including initial conditions, into a matrix system based on algebraic functions. The efficacy and accuracy of this innovative technique are demonstrated through its application to an illustrative example. The results not only showcase the efficiency and precision of our approach but also reveal its capability to yield highly accurate approximations for the budget constraint equation. This study underscores the high accuracy, rapid convergence, and excellent approximation capabilities of the new approach employing Taylor matrix-collocation techniques in solving the budget constraint equation for a group.

Author Statement

The author confirms sole responsibility for the following: study conception and design, data collection, analysis and interpretation of results, and manuscript preparation.

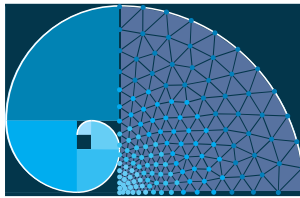
Conflict of Interest

The author declares no conflict of interest.

References

- Achdou, Y., Buera, F. J., Lasry, J. M., Lions, P. L., & Moll, B. (2014). Partial Differential Equation Models in Macroeconomics. *Philosophical Transactions of the Royal Society A: Mathematical, Physical and Engineering Sciences*, 372, 19, 20130397.
- Aydın, Y. (2016). Post Otistik İktisat: İktisat Eğitimi ve Neoklasik İktisat Eleştirisi. *Selçuk Üniversitesi Sosyal Bilimler Enstitüsü Dergisi*, 35, 35-47.
- Bayku, N., & Sezer, M. (2017). Hybrid Taylor-Lucas Collocation Method for Numerical Solution of High-order Pantograph Type Delay Differential Equations with Variables Delays. *Applied Mathematics & Information Sciences*, 11(6), 1795-1801.
- Biçer, K. E., & Yalçınbaş, S. (2016). A Matrix Approach to Solving Hyperbolic Partial Differential Equations Using Bernoulli Polynomials. *Filomat*, 30(4), 993-1000.
- Bilgin, C. (2006). İktisatta Matematiksel Yaklaşım Sorunu. *Sosyoekonomi*, 4(4), 69-84.
- Beed, C., & Kane, O. (1991). What is the Critique of the Mathematization of Economics?. *Kyklos*, 44(4), 581-612.
- Boucekkine, R., Camacho, C., & Fabbri, G. (2013). On the Optimal Control of Some Parabolic Partial Differential Equations Arising in Economics. HAL Id: halshs-00831042.
- Brito, P. B. (2020). Advanced Mathematical Economics, *Doctoral Thesis*, Universidade de Lisboa, Lisbon.
- Burger, M., Caffarelli, L., & Markowich, P. A. (2014). Partial Differential Equation Models in the Socio-economic Sciences. *Philosophical Transactions of the Royal Society A: Mathematical, Physical and Engineering Sciences*, 372(2028), 8, 20130406.
- Chekuri, C., & Kumar, A. (2004). Maximum Coverage Problem with Group Budget Constraints and Applications. *International Workshop on Randomization and Approximation Techniques in Computer Science*. Berlin, Heidelberg: Springer, 72-83.
- Cordier, S., Pareschi, L., & Toscani, G. (2005). On A Kinetic Model for A Simple Market Economy. *Journal of Statistical Physics*, 120, 253-277.
- Çayan, S., Özhan, B. B., & Sezer, M. (2022). An Adaptive Approach for Solving Fourth-order Partial Differential Equations: Algorithm and Applications to Engineering Models. *Computational and Applied Mathematics*, 41(408), 17.
- Çevik, M., & Sezer, M. (2023). Engineering Applications of Polynomial Matrix Method: A Review. *6th International Students Science Congress Proceedings Book*, 206-216.

- Elmacı, D., Yüzbaşı, Ş., & Savaşaneril, N. B. (2022). A Matrix-Collocation Method for Solutions of Singularly Perturbed Differential Equations via Euler Polynomials. *Turkish Journal of Mathematics*, 46(8), 3260-3275.
- Erdem Biçer, K., & Yalçınbaş, S. (2019). Numerical Solution of Telegraph Equation Using Bernoulli Collocation Method. *Proceedings of the National Academy of Sciences, India Section A: Physical Sciences*, 89, 769-775.
- Guo, L., Li, M., & Xu, D. (2017). Approximation Algorithms for Maximum Coverage with Group Budget Constraints. *Combinatorial Optimization and Applications: 11th International Conference, COCOA 2017, Shanghai, China, December 16-18, 2017, Proceedings, Part II 11*, 362-376). Springer International Publishing.
- Gümgüm, S., Savaşaneril, N. B., Kürkçü, Ö. K., & Sezer, M. (2018). A Numerical Technique Based on Lucas Polynomials Together with Standard and Chebyshev-Lobatto Collocation Points for Solving Functional Integro-Differential Equations Involving Variable Delays. *Sakarya University Journal of Science*, 22(6), 1659-1668.
- Kaleci, F., & Buluş, A. (2016). Matematik İktisadi Ele mi Geçiriyor?. *1st International Social Sciences and Muslim Congress: "Hegemony-Counter Hegemony"*.
- Karabakal, N., Bean, J. C., & Lohmann, J. R. (2000). Solving Large Replacement Problems with Budget Constraints. *The Engineering Economist*, 45(4), 290-308.
- Kurt, N., & Çevik, M. (2008). Polynomial Solution of The Single Degree of Freedom System by Taylor Matrix Method. *Mechanics Research Communications*, 35(8), 530-536.
- Kurt, N., & Sezer, M. (2008). Polynomial Solution of High-Order Linear Fredholm Integro-Differential Equations with Constant Coefficients. *Journal of the Franklin Institute*, 345(8), 839-850.
- Moon, I., & Silver, E. A. (2000). The Multi-item Newsvendor Problem with a Budget Constraint and Fixed Ordering Costs. *Journal of the Operational Research Society*, 51, 602-608.
- Pareschi, L., & Toscani, G. (2014). Wealth Distribution and Collective Knowledge: A Boltzmann Approach. *Philosophical Transactions of the Royal Society A: Mathematical, Physical and Engineering Sciences*, 372, 15, 20130396.
- Savaşaneril, N. B. (2023). Lucas Polynomial Solution of The Single Degree of Freedom System. *Scientific Research Communications*, 3(1), 1-10.
- Şahin, R., Ertoğral, K., & Türkbey, O. (2010). A Simulated Annealing Heuristic for The Dynamic Layout Problem with Budget Constraint. *Computers & Industrial Engineering*, 59(2), 308-313.
- Vairaktarakis, G. L. (2000). Robust Multi-item Newsboy Models with a Budget Constraint. *International Journal of Production Economics*, 66(3), 213-226.
- Yücel, K. G. (2022). Politik İktisattan Matematiksel İktisada Yöntem Farklılaşması: Okçuların Yerini Topçular mı Alıyor?. *Akdeniz İİBF Dergisi*, 22(1), 40-56.



An Efficient Index-Based Algorithm for Exact Subgraph Isomorphism on Bipartite Graphs

Mehmet Burak Koca^{1,*} , Fatih Erdoğan Sevilgen² 

¹ Department of Computer Engineering, Gebze Technical University, Kocaeli, Türkiye

² Institute for Data Science and Artificial Intelligence, Boğaziçi University, İstanbul, Türkiye

* Corresponding author: b.koca@gtu.edu.tr

Received: 16.12.2023

Accepted: 13.01.2024

Abstract

Graphs are widely used to represent various real-world networks, but their non-linear nature and size increase pose challenges for efficient analysis. The subgraph isomorphism problem, which involves identifying subgraphs that are isomorphic to a query graph, plays a crucial role in diverse domains. In this paper, we focus on the exact subgraph isomorphism problem in bipartite graphs and propose a novel index-based solution algorithm. Our algorithm leverages triplet structures for graph embedding and uses a multi-level hash map for efficient filtering. We also introduce an optimized solution building process. Experimental results on real-world datasets demonstrate the performance superiority of our algorithm compared to state-of-the-art algorithms, with 2 to 500 times shorter querying times. Our findings suggest that our algorithm is a powerful and efficient solution for exact subgraph isomorphism in bipartite graphs.

Keywords: Subgraph isomorphism; bipartite graphs; index-based

1. Introduction

Graphs serve as essential data structures for modeling various real-world networks such as roadmaps, social networks, protein interactions, and chemical compound structures. The examination of these graph structures plays a pivotal role in understanding the inherent relationships and substructures they encapsulate. Nevertheless, conducting an efficient analysis of these graphs presents formidable challenges, particularly given their non-linear topology and the ongoing growth in dataset sizes.

The subgraph isomorphism (SI) problem is a fundamental technique in graph analysis, widely used in various scientific fields. It involves identifying subgraphs within a target graph that match a specified query graph (Corneil and Gottlieb, 1970). This challenge is common in diverse domains such as protein interaction networks and communication networks, prompting significant efforts to accurately detect these isomorphic structures. However, the SI problem is known for its high complexity, making it challenging to find practical solutions.

Subgraph isomorphism is an NP-complete problem because it is an extension of the maximal clique issue and the challenge of determining whether a graph has a Hamiltonian cycle (Cook, 2023). A Hamiltonian cycle is a cycle that visits each vertex exactly once. In the context of the subgraph isomorphism problem, we are looking for a specific pattern of vertices and edges

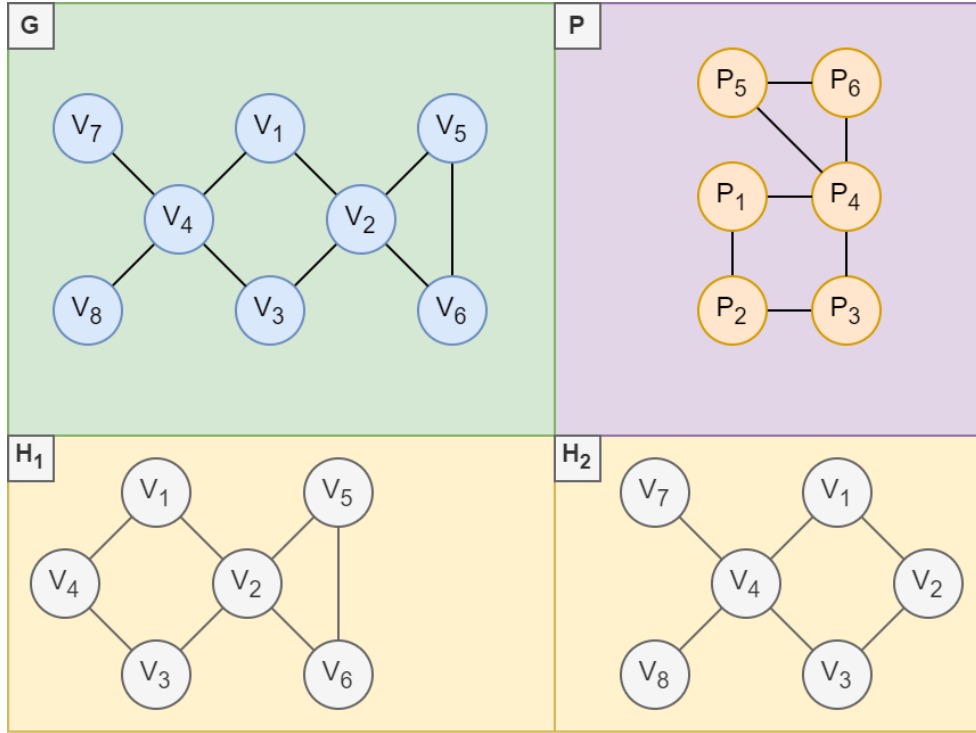


Figure 1. Target graph G , query graph P , exactly isomorphic H_1 and approximately isomorphic H_2 subgraphs of G

within a larger graph that matches the structure of a smaller graph, essentially seeking a subgraph that follows the connectivity pattern of a Hamiltonian cycle. This connection highlights the complexity and generality of the subgraph isomorphism problem.

Moreover, enumerating all isomorphic subgraphs adds an extra layer of difficulty, proving to be more challenging than addressing a singular decision variant (Afrati et al., 2013). Therefore, heuristic algorithms emerge as the main approach for tackling the SI problem.

Two distinct types of subgraph isomorphism problem exist: (I) Exact subgraph isomorphism (Carletti et al., 2015; Ullmann, 1976) and (II) Approximate subgraph isomorphism (Peng et al. 2017). Solutions for the approximate SI problem accommodate for slight variances in vertices, edges, and other semantic properties such as vertex labels, providing an approximate solution. The challenge with exact SI problem, however, rests on finding subgraphs that align flawlessly with the query graph. For example, in Figure 1, subgraph H_1 of G is exactly isomorphic to the query graph P . This isomorphism is achieved by establishing such a mapping between vertices: $P_1 \rightarrow v_1, P_2 \rightarrow v_2, P_3 \rightarrow v_3, P_4 \rightarrow v_4, P_5 \rightarrow v_5, P_6 \rightarrow v_6$. All the edges between any two query vertices, such as $e = (P_1, P_2)$, exists between their corresponding mappings $e' = (v_1, v_2)$. On the other hand, subgraph H_2 requires the presence of an edge (v_7, v_8) to be isomorphic to the query graph P . However, H_2 may be considered as a valid solution while doing approximate querying if the algorithm tolerates a single missing edge.

Solution strategies for the exact SI problem fall into two primary categories: (I) Index-based algorithms and (II) Constraint-based algorithms. In constraint-based algorithms (Cordella et al., 2004; Han, Lee, & Lee, 2013; He and Singh, 2008; Shang et al. 2008; Ullmann, 1976), an initial vertex is recursively extended through the addition of relevant neighbor vertices. This process when suitable vertices for branching are exhausted of the complete isomorphic subgraph is found. On the other hand, index-based algorithms

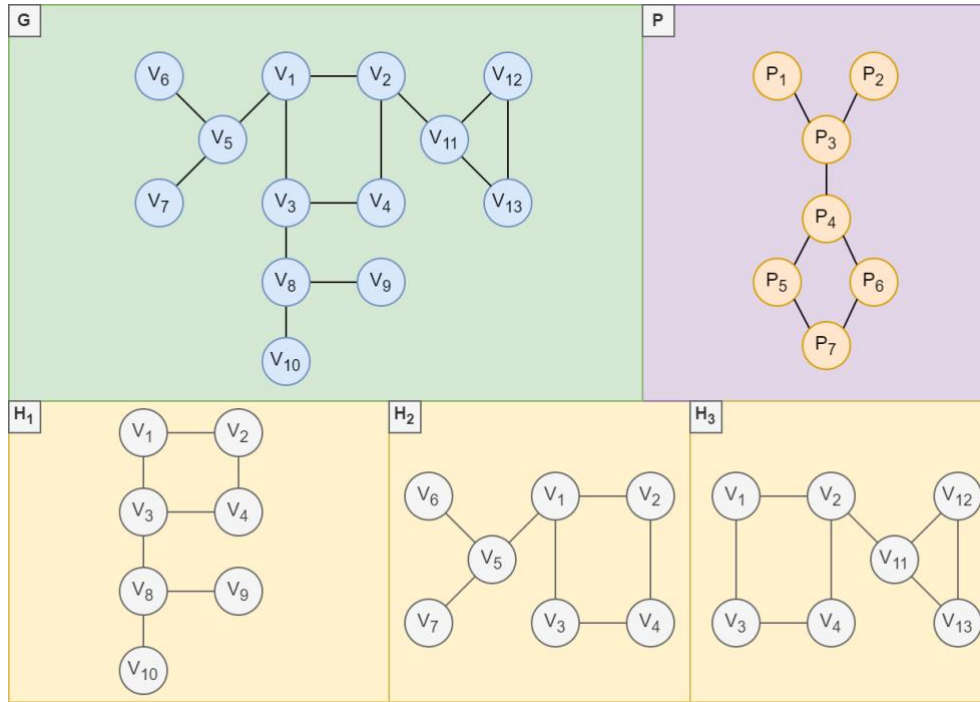


Figure 2. Target Graph G , Query Graph P , isomorphic subgraphs H_1, H_2 and non-isomorphic subgraph H_3

(Bonnici et al., 2010; Cheng et al., 2007; Kim et al., 2023) serve to improve the efficiency when dealing with large and dense graphs through a divide and filter approach. These algorithms manipulate sub regions of the query graph correlating to sub regions of the target graph. The idea behind the index-based algorithms include embedding the target graph into sub regions, filtering required embeddings through the query graph, and building partial solutions.

Despite these efforts, data sources' rapid expansion places immense demands on these algorithms for efficiency and resourcefulness, especially in maintaining efficiency across all graph types in SI problems. There are such algorithms (Peng et al., 2015) resort to hardware technologies and parallel programming in handling large graphs. However, this approach has its limitations, especially when financial resources limit the tasks performed and thus not a practical solution to the problem. By tailoring the solutions to a given graph type, performance can be substantially enhanced (Koca and Sevilgen, 2019).

Bipartite graphs prove its significance in modeling related networks like pathogen-host protein-protein relation networks or customer-product recommendation networks. Thus, an efficient solution to the SI problem on bipartite graphs is critical for revealing latent biological or social patterns in wide scale graphs, often encompassing tens of thousands of vertices.

In this study a novel index-based solution algorithm is proposed for the exact subgraph isomorphism problem on bipartite graphs. The algorithm consists of three primary steps consistent with index-based approaches: Firstly, embedding the target graph G using P_3 (triplet) structures and storing them in a hash-map. Secondly, embedding the query graph P and filtering the hash-map to identify suitable candidate embeddings for P . Finally, joining the candidate triplets to generate the exact solutions.

The proposed algorithm's performance is compared against existing state-of-the-art algorithms based on the execution times. Our algorithm achieved 2 to 500 times shorter querying times than its competitors. These results demonstrate that our algorithm

outperforms state-of-the-art algorithms developed for general graphs in solving the exact subgraph isomorphism problem on bipartite graphs.

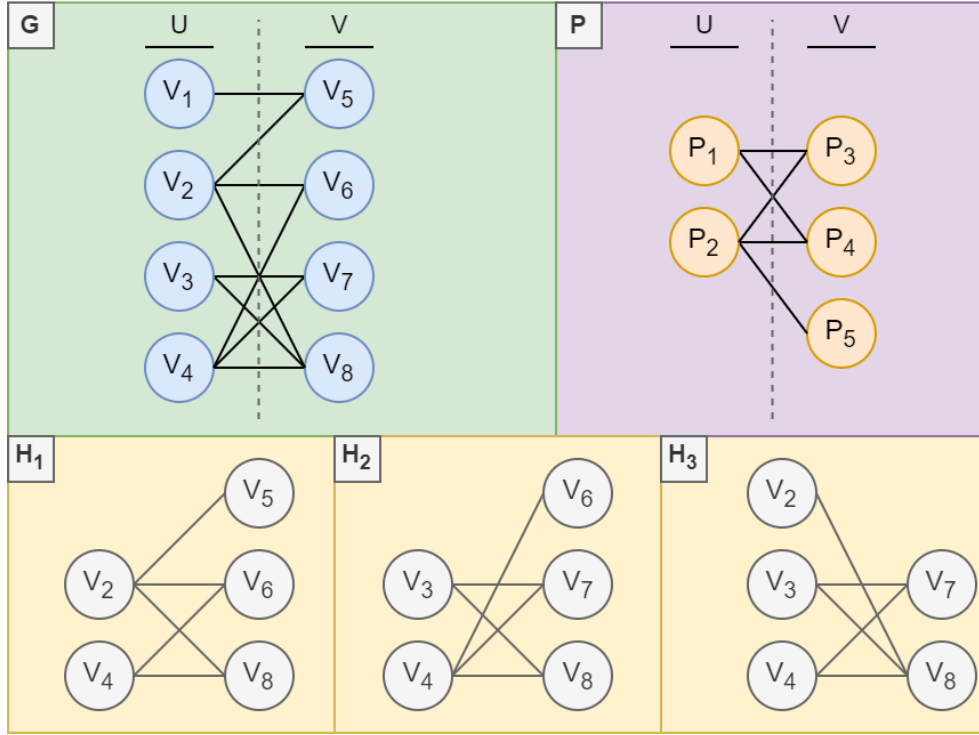


Figure 3. Target bipartite graph G , query bipartite graph P , the subgraphs that bipartite isomorphic to P H_1 , H_2 and non-isomorphic bipartite subgraph H_3

2. Preliminaries

The fundamental definitions are presented to enhance the understanding of the study. The subgraph isomorphism (SI) problem is an extension of the graph isomorphism problem.

Definition 1 (Graph isomorphism): $G_1 = (V, E)$ and $G_2 = (V', E')$ are given two graphs. If there is a surjective function A from G_1 to G_2 , $A: G_1 \rightarrow G_2$ such that, $\forall v \in V, A(v) \in V'$ and $\forall e = (v_1, v_2) \in E, A(e) = (A(v_1), A(v_2)) \in E'$, then G_1 and G_2 are isomorphic graphs, $G_1 \cong G_2$.

For isomorphic graphs, there is at least one mapping that allows the vertices of one graph to be aligned with the vertices of the other graph, preserving their adjacency relationships. For instance, in Figure 2, graphs H_1 and H_2 are isomorphic graphs. This isomorphism can be achieved by mapping the vertices $V_1, V_2, V_3, V_4, V_8, V_9, V_{10}$ of H_1 to $V_2, V_4, V_1, V_3, V_5, V_6, V_7$, respectively, in H_2 .

Definition 2 (Subgraph - induced subgraph): $G = (V, E)$ is a given graph, any substructure $H = (V', E')$ of G such as $V' \subseteq V$ and $E' \subseteq E \cap (V' \times V')$ is a subgraph of G . If E' contains all the edges in E that are between vertices in the set V' that is $E' = E \cap (V' \times V')$ then, H is an induced subgraph of G .

In the context of the SI problem, it is crucial to distinguish between the terms subgraph and induced subgraph. The solution algorithm may not consider extra edges when searching for non-induced subgraphs. For instance, in Figure 2, all three subgraphs H_1 , H_2 , and H_3 are isomorphic to P . However, H_3 is not a valid solution for an algorithm targeting induced subgraphs of G . This study focuses on finding isomorphic induced subgraphs; hence, the term subgraph is used to refer to induced subgraphs in this paper.

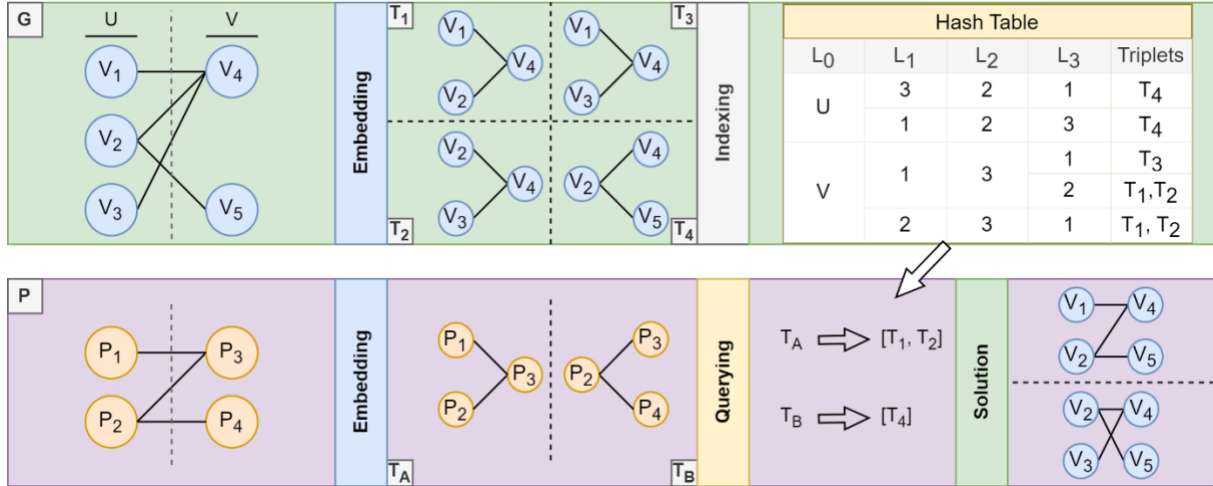


Figure 4. The workflow of the proposed subgraph isomorphism algorithm is illustrated. The target graph is embedded into triplets, and these triplets are stored in a multi-level key hash map (top). During the search for isomorphic subgraphs using a query graph, the query is also initially embedded into triplets. Subsequently, the suitable candidates for each query triplet are selected from the hash map through a filtering process. Finally, the exact solutions are generated by joining candidate triplets while taking into account the connections of the triplets within the query graph (bottom)

Definition 3 (Subgraph isomorphism problem): $G = (V, E)$ and $P = (V', E')$ are given two graphs where $|V'| \leq |V|$, $|E'| \leq |E|$. The subgraph isomorphism problem is finding all subgraphs H in the G such that $H \cong P$.

The graph G in Figure 2 has two subgraphs H_1 and H_2 that isomorphic to P . However, H_3 is not isomorphic to P because the edge $e = (v_{12}, v_{13})$ makes any mapping possible.

Definition 4 (Bipartite graph): $G = (U, V, E)$ is a bipartite graph where U and V are two disjoint and independent vertex sets and E is edge set that consists of edges $e = (u, v)$ where u is in U and v is in V .

In Figure 3, all the graphs depicted are bipartite graphs. Bipartite graphs are characterized by having two disjoint and independent vertex sets, denoted as U and V , as shown in the figure. In a bipartite graph, every edge connects two vertices that belong to different sets, meaning there are no edges within the same set. This property distinguishes bipartite graphs from general graphs where edges can connect any pair of vertices.

Definition 5 (Bipartite isomorphism): $G = (U, V, E)$ and $G' = (U', V', E')$ are given two bipartite graphs. If there is a bijection $I: (V \rightarrow V', U \rightarrow U')$ such that $\forall u \in U, v \in V$ and $e = (u, v) \in E; I(u) \in U', I(v) \in V'$ and $(I(u), I(v)) \in E'$ then, G and G' are isomorphic bipartite graphs.

Indeed, in bipartite graphs, the partitioning of vertices into different partite sets is crucial for bipartite isomorphism. The partite sets represent distinct groups of objects, such as clients-servers or human protein-virus protein, and the relationships between them are captured by the edges connecting vertices from different sets. Consequently, mirrored subgraphs, where the partite sets are swapped, do not convey the same meaning.

Figure 3 provides an example of bipartite isomorphic graphs. The graphs H_1 and H_2 are bipartite isomorphic since they exhibit the same vertex-partitioning pattern and maintain the relationships between the two partite sets. However, graph H_3 is not bipartite isomorphic to H_1 and H_2 , even though all three graphs are isomorphic in the general sense.

Definition 6 (SI problem in bipartite graphs): $G = (U, V, E)$ and $G' = (U', V', E')$ are given two bipartite graphs such that $|U| \leq |U'|$, $|V| \leq |V'|$, $|E| \leq |E'|$. The SI problem on the bipartite graphs is finding all subgraphs H of G' that are bipartite isomorphic to G .

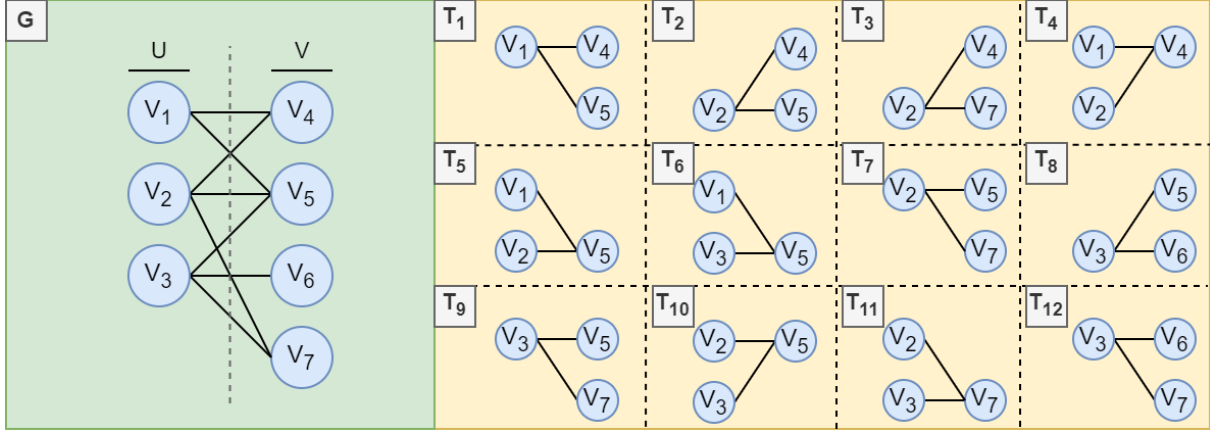


Figure 5. The target graph G and its triplet embeddings

The subgraph isomorphism problem on bipartite graphs is almost the same as the SI problem. However, only bipartite isomorphic subgraphs are considered valid solutions. In Figure 3, the subgraphs H_1 and H_2 are in the solution set of the SI problem for G and P . However, H_3 is not bipartite isomorphic to P because the vertex V_2 , which is the mapping of P_5 , is in the set V instead of the set U .

As all essential definitions are presented, In Section 3, our novel algorithm is introduced, and all the sub-processes are explained in detail. Moreover, the advantages of the bipartite structure are explicitly described for each sub-process. The experimental results are given and discussed in Section 4. Finally, our conclusions regarding this study are presented in Section 5.

3. Methodology

Our algorithm utilizes an enumerate, filter, and build approach, which is commonly employed in state-of-the-art algorithms for solving the SI problem. The workflow of the algorithm is illustrated in Figure 4. Initially, the target graph G is embedded into triplets and subsequently stored within a multi-level hash map. This hash map is then employed to fulfill subgraph querying requests. During the SI search phase, the query graph is also embedded into triplets as a preliminary step. Relevant triplets within G are extracted through hash map queries to establish potential matches for the query graph's triplets. Ultimately, these appropriate candidates are joined together, accounting for the structural attributes of the query graph, with the aim of constructing exactly isomorphic subgraphs with the query. These procedures have been specifically adapted for bipartite graphs to enhance the performance of SI searches for this graph type. The details of how the proposed algorithm leverages the bipartite structure of the target graph in each procedure and elucidates the resulting improvements in performance.

3.1. Embedding

Many state-of-the-art algorithms addressing the SI problem primarily focus on enhancing the detection of sub regions within the target graph that may potentially contain the query subgraph. These algorithms often employ graph embedding techniques to enumerate the sub-

parts of the target graph. Among the available graph embedding techniques, vertex embedding techniques are widely used due to their ability to provide valuable local information that can effectively aid in sub region filtering. These techniques make use of structural properties of vertices, such as vertex degrees, the count of k -length neighbors, and neighbors' degrees. For example, in (Tian and Patel, 2008), a vertex embedding technique is employed that stores a vector for each neighbor of a vertex. This vector incorporates information such as degree, neighbor count, label, and the sum of neighbor degrees. By utilizing such embedding techniques, algorithms can access highly informative and detailed local information for all vertices, thereby improving the accuracy of the filtering process.

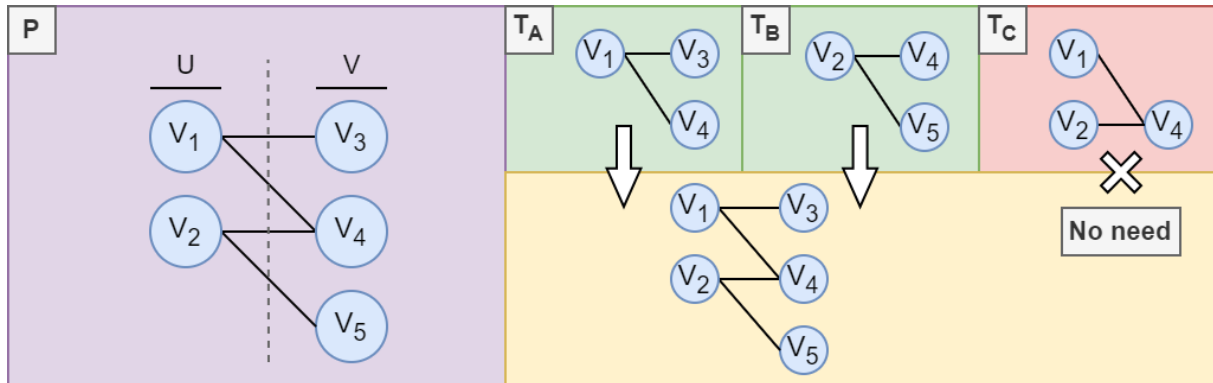


Figure 6. An example of generating solution building triplet set for the query graph P . The T_A and T_B triplets are sufficient to build query graph whereas the T_C triplet is unnecessary

The vertex embedding techniques can be inefficient when applied to huge target graphs. Building solutions by using the filtered candidates can become more challenging since the algorithm needs to extend partial solutions by one vertex at each step. As the number of partial solutions exponentially grows with each step, these techniques can result in being inoperative due to execution times for generating exact solutions.

To address these challenges, methods involve embedding more than one vertices together (Chen et al., 2007; Hong et al., 2015), as opposed to individually embedding vertices. These vertex groups often represent common sub structures such as cycles, paths, or other patterns. By considering these groups, the number of embeddings is reduced, leading to a smaller search space and enabling faster candidate filtering for parts of the query graph. Furthermore, since the embeddings consist of multiple components and the algorithm can add multiple components to partial solutions, the number of steps required for the solution process has the potential to decrease.

In this study, a path embedding technique is used instead of vertex embedding due to the mentioned problems. The length of the path, L , has been optimized since it is crucial for the performance of the embedding technique. If L is set to be too large, the embeddings have high resolution, making the filtering process more demanding. However, long paths lead to complicate the handling of complete solutions. In some cases, the solutions may not be feasible to handle because the algorithm may lack smaller sub structures necessary to construct a complete solution. On the other hand, when the path length is too small, it can lead to problems, as explained for single vertex embedding techniques. Various constraints are taken into account to optimize this parameter for bipartite graphs.

Initially, a path length of 1, denoted as $L = 1$ or P_2 is considered. Such path consisting of two vertices connected by a single edge. This sub structure is promising for embedding bipartite

graphs because each embedding consists of two vertices that hosted in different partitions. Such an information can be used for efficient filtering. However, in an undirected complete bipartite graph with partitions of sizes k and m , the total number of embeddings is equal to $k * m$. Since the solution algorithm benefits from the partitions of vertices in the embeddings, the partial solutions can be expanded only by suitable candidates that belong to the same partition order as their corresponding query embeddings.

The $L = 2$ structure, also known as P_3 or triplet, is evaluated since it also potentially suitable for embedding bipartite graphs. Each triplet consists of two tail vertices in one partition and one head vertex in the other partition, regardless of their adjacencies. While the number of embeddings are increased when using P_3 instead of P_2 , triplets offers an opportunity to further enhance filtering and solution building performance compared to P_2 . Triplets can handle three vertices and two edges simultaneously, leveraging the same structural information as P_2 .

The $L = 3$ paths are also considered to explore if P_4 structures offer any additional benefits compared to triplets. However, it seems that P_4 structures provides no additional information specific to the bipartite structure. In fact, they can be precisely represented using two triplets. Therefore, it is concluded that values of L greater than 2 are not suitable for the bipartite graphs. Moreover, P_4 structures and longer paths have the potential to create loops, which must be checked by the algorithm to ensure compliance with the conditions of the induced subgraph isomorphism problem. However, such a control mechanism would add computational load to the algorithm. Hence, it is determined that the most suitable path length is 2 for bipartite graphs, as any path longer than 2 would decrease the algorithm's performance.

The embedding path structure can be expanded without altering the parameter L by incorporating three neighbors of the head vertex. This structure, known as the claw, contains the same information as triplets but allows for an increase in the number of components at each step of partial solution extension. However, the concatenation process of two claws takes more time than triplet concatenation due to the additional vertex that needs to be checked for suitability with the current partial solution. Another challenge with the claw structure arises during the generation of embeddings, as the presence of an extra vertex increases the number of embeddings. This increase in the number of embeddings can significantly impact the performance of the embedding and filtering processes.

Several of these structures have been tested, and the comprehensive experimental results are presented in the fourth part. The performance results obtained support our theoretical assumptions, indicating that triplets are the optimal data structure for embedding bipartite graphs.

3.2. Filtering

The performance of the algorithm heavily relies on the filtering process, which is as important as the embedding process. The filtering process starts by enumerating triplets in the query graph using the same embedding method used in the target graph. The embeddings of the target graph are then filtered to identify candidates for the query triplets based on their structural properties. While query graphs typically consist of a few triplets, the number of embeddings in the target graph can be in the millions, making effective filtering techniques essential to maintain the algorithm's efficiency.

Our algorithm leverages vertex degrees and partite information for efficient filtering. The triplet structure provides favorable locality for the solution building process. Since exact solutions require identical adjacency relations, vertex degrees serve as a powerful indicator for identifying suitable candidates.

Incorporating partite information into the algorithm ensures the elimination of unsuitable candidates during the solution building process, which can be computationally expensive. Furthermore, the partite information plays a crucial role in generating exact solutions in bipartite graphs, preventing the algorithm from producing mirrored solutions where all vertices are placed in the opposite partition.

Table 1. The hash-map of embeddings in Figure 5.

Level-0	Level-1	Level-2	Level-3	Triplet List
P1	1	3	2	T12
			3	T8
		2	3	T1
	2	3	1	T12
			2	T3
			3	T2, T7, T9
	3	2	2	T1
		3	1	T8
			2	T2, T7, T9
P2	2	2	3	T4
		3	3	T5, T6
	3	2	2	T4
			3	T11
		3	2	T5, T6
			3	T10

The embeddings of the target graph, as shown in Figure 6, are stored in a multi-level hash map similar to Table 1. This hash map enables efficient filtering with $O(1)$ access time. Pushing the embeddings into the hash map requires a total execution time of $O(n)$ due to the nature of map data structures ($O(1)$ per insertion $\times n$ embeddings).

The filtering process aims to avoid complex search operations and provide $O(1)$ or, at most, $k \times O(1)$ access time, ensuring that the keys satisfy the filtering constraints to a large extent.

The level-0 key of the map has two possible values, P_1 and P_2 , representing the two partitions of the bipartite graph. The partite of a triplet is determined by the partite of its head vertex. For example, if the head vertex of a query triplet belongs to partition 1, the candidates for that triplet will be limited to the embeddings with a level-0 key value of P_1 . By filtering the embeddings based on their partite information at the level-0 key, the algorithm significantly reduces the search space.

The level-1, level-2, and level-3 keys in the hash map store the vertex degrees of the triplets. Level-1 corresponds to the degrees of the left tail vertices, level-2 corresponds to the degrees of the head vertices, and level-3 corresponds to the degrees of the right tail vertices. It should be noted that the order of the left and right tails is interchangeable.

During the filtering process, it is necessary to consider the mirrored values of the level-1 and level-3 keys. To avoid the additional computational load of handling mirrored values, each embedding is stored in the hash map with both the regular key combination and an alternate key combination where the level-1 and level-3 keys are interchanged (as shown in Table 1, T_1). Although this approach doubles the memory usage for storing the embeddings, it reduces the CPU requirements of the filtering process.

In the filtering process, it is important to account for the presence of additional edges between vertices that are not part of the sub region in an isomorphic subgraph. These extra edges do not violate the definition of exact subgraph isomorphism but can increase the vertex degrees. To prevent filtering out valid candidates, the algorithm filters only the triplets that have a lower vertex degree for each key level. For example, if the left tail vertex of the query triplet has a degree of d , then only triplets with a vertex degree equal to or greater than d for the left tail vertex will remain for the next levels.

The elimination process involves searching the keys of the hash map, resulting in a filtering process that takes more than $O(1)$ execution time. However, since there can be at most n different degrees in a graph, the filtering process takes $3 * n * O(1) = O(n)$ execution time in the worst case. In practical scenarios, the degree diversity is typically much less than the number of vertices, so the filtering process is usually completed quickly.

By default, the proposed algorithm doesn't consider vertex labels or edge directions, as the focus is on solving the subgraph isomorphism problem in bipartite graphs in the most general form. However, the algorithm can support the inclusion of these constraints by adding additional levels to the data structure. For example, vertex labels can be incorporated into the filtering process by adding three distinct keys to the data structure, allowing the checking of triplet vertices based on their labels before considering their compatibility with vertex degrees. Similarly, the algorithm can be adapted to support inexact searches by adding one or two levels for vertex labels. The absence of keys for the labels provides flexibility, enabling researchers or end-users to customize the algorithm according to their specific needs.

3.3. Building solution

The process of building exact solutions involves joining candidates of query triplets together to generate partial solutions. These partial solutions are expanded by adding exactly one candidate on each step. If a partial solution cannot be expanded and is isomorphic to the query graph, it is considered a valid exact solution. However, if a partial solution has missing vertices and there is no possibility for further expansion, it is eliminated.

When a candidate joins a partial solution, it is done while considering the adjacency relations of its owning triplet. The partial solution represents a mapping of a sub region in the query graph, and some vertices of the owner triplet may already be mapped in the current partial solution. This means that some vertices in the partial solution must match the vertices of the new candidate. Therefore, partial solutions can be expanded with candidates that share the same adjacency relation between their owner triplet and the mapped sub-region. By considering these adjacency relations, the algorithm ensures that the candidate being added is compatible with the existing mapping.

This step-by-step expansion and mapping process allows the algorithm to gradually build exact solutions by iteratively adding compatible candidates to the partial solutions, ultimately leading to a complete and valid mapping of the query graph.

The joining process of two triplets involves considering common vertices between them. Candidates of one triplet can generate partial solutions by joining with candidates of the other triplet if they share a common vertex. Some candidates may not be compatible due to mismatched mappings. Joining triplets allows the algorithm to gradually build partial solutions by expanding them with compatible candidates.

Not all triplets in the query graph are necessary for building complete solutions. Triplets whose vertices have already been mapped in the current partial solution do not contribute

additional information. Joining such triplets with existing partial solutions does not generate new solutions or eliminate existing ones.

Selecting the optimal set of triplets, known as the Solution Building Triplet Set (BTS), is crucial for algorithm performance. The optimal BTS minimizes the number of joining processes required, as joining triplets can be computationally expensive. However, finding the optimal BTS is challenging, and there is no greedy method that guarantees an optimal solution. Brute-force algorithms can be used to generate all possible BTSs and estimate their join count based on candidate numbers. While this approach can yield efficient BTSs, it becomes impractical for larger BTS sizes due to excessively long execution times.

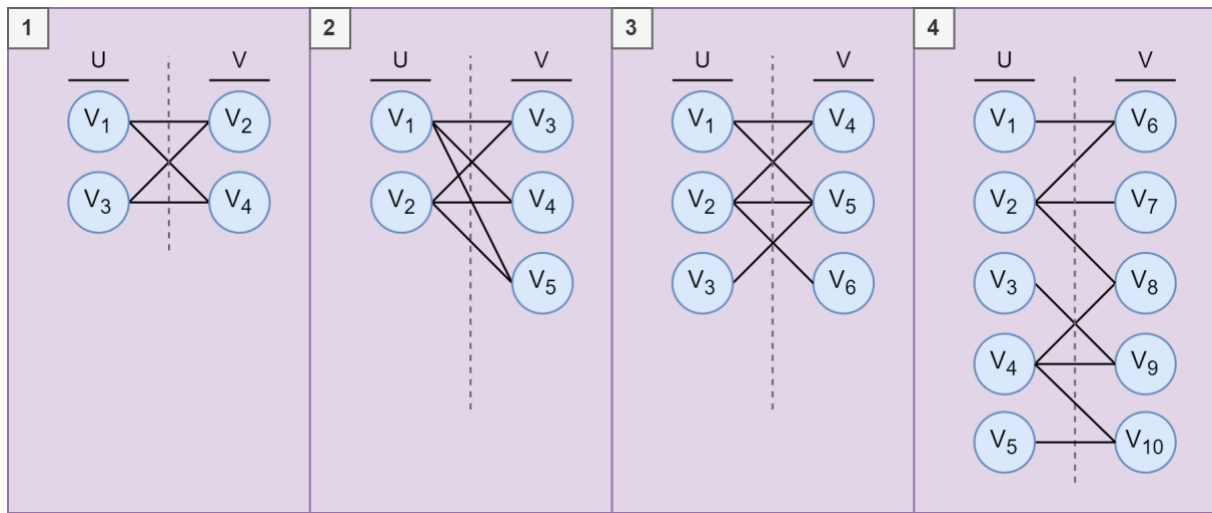


Figure 7. The four query graphs used in both experiments

The proposed greedy algorithm aims to find efficient Solution Building Triplet Sets (BTS) in a time-efficient manner. The algorithm sorts query triplets based on the number of candidates they have, with the triplet having the fewest candidates added as the first triplet in the BTS. Privileged triplets are marked and added to the BTS based on the number of candidates they have. Triplets with more uncontained edges become privileged for each step.

The ordering of triplets within the BTS is also optimized to reduce the number of unsuitable partial solutions. The triplet with the highest number of candidates is placed at the head of the ordered BTS. The next triplet is selected from the triplets that have more contained vertices by the ordered BTS, with priority given to triplets with the highest number of candidates. This selection reduces the generation of unsuitable partial solutions and decreases the number of partial solutions for subsequent steps.

By utilizing these greedy approaches, the algorithm aims to minimize unnecessary computations by reducing the number of joins and unsuitable partial solutions, ultimately improving the performance of building exact solutions.

4. Results and Discussions

4.1. Experimental Setup

The performance of the proposed algorithm is assessed both with and without the enhancements suggested for addressing sub-problems. Additionally, the empirically best

version of the algorithm is compared against state-of-the-art subgraph isomorphism algorithms to demonstrate its efficiency. The execution time of the querying process of algorithms is used as the performance metric. Both the proposed algorithm and its competitors are implemented in the Python programming language. The comparative algorithms are evaluated using their publicly accessible implementations. The experiments are carried out on a computer equipped with a 3.3 GHz i7 CPU and 16 GB of RAM, running the Ubuntu operating system.

4.2. BTS Selection Methods Comparison

Two distinct experimental setups were conducted to assess improvements in determining the reconstruction strategy for the query graph solution. Initially, the selection algorithms of the BTS were evaluated in terms of the time required to calculate BTS and the number of joins needed to identify all solutions using the computed BTS. Subsequently, the algorithms for ordering BTS to construct solutions were assessed based on their execution time for generating solutions.

The protein-protein interaction network between Adenoviridae proteins and Human proteins obtained from PHISTO (Durmuş Tekir et al., 2013). Database is used as target graph in both experiments. This interaction graph comprises 324 vertices with 379 interactions among them. The query graphs, as depicted in Figure 7, were employed in both experiments to evaluate how the tested algorithms perform with query graphs of varying sizes. Each individual test was repeated 10 times, and the average execution times are presented.

The greedily selection approach for generating BTS was compared with the brute-force selection algorithm, revealing that the greedy algorithm is 10 to 1000 times faster than its alternative, as indicated by the experimental results. This substantial difference in BTS selection holds particular significance in fields that frequently encounter changing query graphs. The results suggest that the brute-force approach tends to become impractical as the size of the query graphs increases, while the greedy approach exhibits greater resilience to such increases in query graph size. However, it is worth noting that BTS selection is a one-time process, and the brute-force approach may still be preferable in situations where time constraints are not a primary concern, particularly in fields that consistently encounter the same query graphs.

The algorithms are further assessed based on the quality of the BTS they generate. The performance of a BTS is gauged by comparing the total number of joins required to generate all solutions using that BTS. The results, as presented in Table 2, indicate that the greedy algorithm largely produced optimal solutions for three out of the four query graphs. However, for query 4, the brute-force algorithm's optimal solution outperformed the BTS generated by the greedy algorithm in terms of join count. It is important to note that the greedy algorithm may increase query time due to the growing number of join operations needed for constructing solutions. Therefore, the choice of BTS selection method should be made based on the frequency of query changes within the specific field of application.

Table 2. Performance comparison of reconstruction set selection algorithms.

Algorithm		Query (1)	Query (2)	Query (3)	Query (4)
Greedy	Exec time	3.17×10^{-5}	8.37×10^{-5}	8.20×10^{-5}	1.15×10^{-4}
	# of Joins	73984	458480	122600	37550538
Brute-Force	Exec time	1.48×10^{-4}	1.54×10^{-2}	6.56×10^{-3}	7.38×10^{-1}
	# of Joins	73984	458480	122600	20959821

The evaluation of the algorithms for ordering the triplets within the BTS is conducted by measuring the query execution times incurred when building solutions by joining the triplets in the order in which they were generated. There are two types of strategies for ordering BTS, distinguished by whether they take into account the connection with the current partial query when selecting the next triplet for ordering. Additionally, various approaches for selecting the most advantageous triplet among the current candidates can be explored. In this study, we tested the strategy of selecting the next triplet based on the number of candidates it has in the target graph.

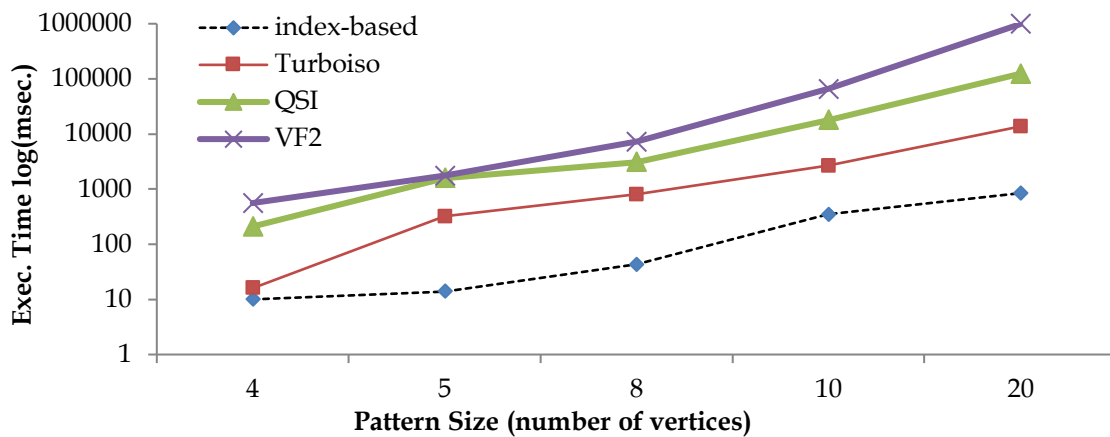


Figure 8. Performance of comparison algorithms in subgraph isomorphism search on the protein-protein interaction graph of Poxviridae. The proposed algorithm consistently outperforms all other algorithms in the search for all subgraphs

The experimental results presented in Table 3 revealed that the strategy of selecting the next triplet from those that don't break connectivity exhibited superior performance when compared to competing strategy. Additionally, giving priority to triplets with the highest number of candidates in the target graph led to a remarkable enhancement in performance. As a result, the greedy approach was employed for candidate selection within the BTS in subsequent experiments. Furthermore, the selection of the next triplet during solution construction was determined by choosing the triplet with the maximum number of candidates from among the remaining triplets connected with the current partial solution.

Table 3. Comparative execution times of querying with various BTS ordering algorithms.

Approach	Candid count	Query (1)	Query (2)	Query (3)	Query (4)
Connected	Maximum	1.22×10^{-5}	5.41×10^{-2}	8.21×10^{-1}	2.47
	Minimum	9.05×10^{-4}	9.17×10^{-1}	2.25	98.25
Not connected	Maximum	1.10×10^{-5}	4.67	103.25	173.10
	Minimum	1.51×10^{-5}	1.21	19.37	125.92

4.3. Comparing With the State-of-art Methods

The proposed index-based solution method is compared with state-of-the-art subgraph isomorphism algorithms VF2 (Cordella et al., 2004), QuickSI (Shang et al., 2008) and Turbo^{iso} (Han et al., 2013). Two experiments are designed to evaluate the performance of our algorithm in bipartite graphs. In the first experiment, the performance of the algorithms is evaluated by comparing their execution times with queries of varying sizes. The protein-protein interaction dataset of Poxviridae serve as the target graph for these experiments, comprising 210 proteins and 454 interactions among them. The query graphs depicted in Figure 7 are employed in experiments. Furthermore, a larger query graph, represented as a complete bipartite graph with 20 vertices, is also utilized.

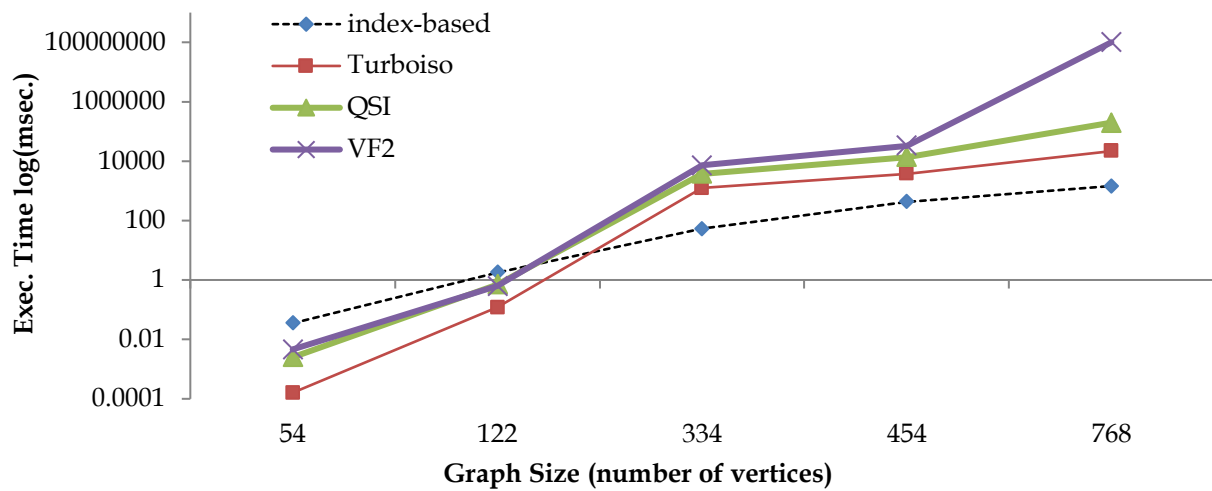


Figure 9. Performance comparison of state-of-the-art algorithms on different target graphs.

The results indicate that our algorithm outperforms others when the target graph size exceeds a few hundred vertices. However, in small graphs, the algorithm exhibits poorer performance, primarily due to its preprocessing step

The tests are conducted ten times for each algorithm across all five query graphs. The resultings, as depicted in Figure 8, demonstrated the superior performance of the proposed algorithm, with notable improvements ranging from 2 to 500 times shorter querying times. It is worth noting that our algorithm consistently exhibited the best performance across all query sizes, while all methods exhibited acceptable execution times in the case of small query graphs. Particularly, the Turbo^{iso} algorithm displayed the second-best performance across all query graphs. As anticipated, the VF2 algorithm exhibited the poorest performance, in line with previous studies that have established the superior performance of both Turbo^{iso} and QuickSI. Nevertheless, it remains valuable to present VF2's performance as a reference point for baseline performance assessment.

In contrast to the performance in small query graphs, it is evident that the execution times of the algorithms increase quadratically with the query sizes, whereas our algorithm demonstrates a linear increase. This highlights the sustained usability of the proposed algorithm for larger query graphs, especially as its competitors become impractical for such scenarios. Consequently, the performance results showcase the algorithm's superiority, underscoring its robustness in the face of expanding query sizes.

We also assessed the algorithm's execution times on target graphs with varying sizes, and the performance results are depicted in Figure 9. These graphs encompass protein-protein interactions involving five different viruses and their proteins in relation to human proteins. Our algorithm exhibited poor performance than its competitors on small graphs containing 120 or fewer vertices, primarily due to its preprocessing step for index generation. However, the results illustrate that our algorithm demonstrates superior performance when the size of the target graphs exceeds a few hundred vertices.

The proposed algorithm exhibits greater robustness for growing target graph sizes compared to all other algorithms in the comparison. However, Turbo^{iso} and QuickSI demonstrate greater resilience to increasing target graph sizes than to increases in query sizes. VF2 shows the poorest performance and robustness. The experimental results provide compelling evidence that our index-based algorithm stands as a prominent solution for addressing the subgraph isomorphism problem within bipartite graphs.

5. Conclusions

Our study presents substantial contributions to the field of subgraph isomorphism in bipartite graphs. We have addressed the pivotal challenge of identifying subgraphs that are isomorphic to a given query graph, acknowledging the complexities stemming from the non-linear nature of graphs and the ever-expanding size of datasets.

To address the exact subgraph isomorphism problem, we have introduced a novel index-based solution algorithm tailored specifically for bipartite graphs. Our approach employs a divide and filter strategy; the target graph is embedded using triplet structures and subsequently filtered based on vertex degrees and partitions of search graph. This approach significantly reduces the search space and enhances the overall efficiency of the algorithm.

Our experimental results conclusively demonstrate the superiority of our index-based algorithm when compared to state-of-the-art methods. It consistently achieves 2 to 500 times shorter querying times, underscoring its effectiveness and scalability for medium to large bipartite graphs.

Furthermore, our study has underscored the critical importance of reconstruction set selection in achieving computational efficiency. The careful selection of a subset of triplets that minimizes the number of join operations has proven to be highly effective for improving overall algorithm performance. Additionally, the ordering of the reconstruction set, starting with triplets featuring the maximum number of candidates and selecting neighboring triplets with high candidate counts, has proven to be a valuable strategy. Nonetheless, there is still room for enhancing the algorithm's performance by refining the ordering strategy. Additionally, exploring the possibility of joining multiple triplets that share intersecting join processes may be worthwhile, as it holds the potential to reduce solution construction time.

In summary, our study provides a comprehensive evaluation of different algorithms for solving the exact subgraph isomorphism problem on bipartite graphs. The proposed index-based algorithm stands out for its remarkable efficiency and effectiveness, establishing itself as a superior solution for large-scale bipartite graphs like pathogen-host protein-protein interaction networks.

Acknowledgements

We would like to thank Dr. Saliha Durmuş and Merve Yaşar Semiz for their contribution to setting up experiments and providing helpful feedback on our study.

Author Statement

The authors confirm their contributions to the paper as follows: algorithm conception and design: M.B. Koca, F.E. Sevilgen; implementation and experimentation: M.B. Koca; analysis of experimental results: M.B. Koca, F.E. Sevilgen; draft manuscript preparation: M.B. Koca, F.E. Sevilgen. All authors reviewed the results and approved the final version of the manuscript.

Conflict of Interest

The authors declare no conflict of interest.

References

- Afrati, F. N., Fotakis, D., & Ullman, J. D. (2013). Enumerating Subgraph Instances Using Map-Reduce. *2013 IEEE 29th International Conference on Data Engineering (ICDE)*, 62–73.
- Bonnici, V., Ferro, A., Giugno, R., Pulvirenti, A., & Shasha, D. (2010). Enhancing Graph Database Indexing by Suffix Tree Structure. In T. M. H. Dijkstra, E. Tsivtsivadze, E. Marchiori, & T. Heskes (Eds.), *Pattern Recognition in Bioinformatics*. Berlin, Heidelberg: Springer.
- Carletti, V., Foggia, P., & Vento, M. (2015). VF2 Plus: An Improved Version of VF2 for Biological Graphs. In C.-L. Liu, B. Luo, W. G. Kropatsch, & J. Cheng (Eds.), *Graph-Based Representations in Pattern Recognition*. Cham: Springer International Publishing.
- Chen, C., Yan, X., Yu, P. S., Han, J., Zhang, D.-Q., & Gu, X. (2007). Towards Graph Containment Search and Indexing. *Proceedings of the 33rd International Conference on Very Large Data Bases*, 926–937. Vienna, Austria: VLDB Endowment.
- Cheng, J., Ke, Y., Ng, W., & Lu, A. (2007). Fg-index: Towards Verification-free Query Processing on Graph Databases. *Proceedings of the 2007 ACM SIGMOD International Conference on Management of Data*, 857–872. New York, NY, USA: Association for Computing Machinery.
- Cook, S. A. (2023). The Complexity of Theorem-Proving Procedures. In *Logic, Automata, and Computational Complexity: The Works of Stephen A. Cook* (1st ed.). New York, NY, USA: Association for Computing Machinery.
- Cordella, L. P., Foggia, P., Sansone, C., & Vento, M. (2004). A (Sub)graph Isomorphism Algorithm for Matching Large Graphs. *IEEE Transactions on Pattern Analysis and Machine Intelligence*, 26(10), 1367–1372.
- Corneil, D. G., & Gotlieb, C. C. (1970). An Efficient Algorithm for Graph Isomorphism. *Journal of the ACM*, 17(1), 51–64.
- Durmuş Tekir, S., Çakır, T., Ardiç, E., Sayılırbaş, A. S., Konuk, G., Konuk, M., Ülgen, K. Ö. (2013). PHISTO: Pathogen-host interaction search tool. *Bioinformatics*, 29(10), 1357–1358.
- Han, W.-S., Lee, J., & Lee, J.-H. (2013). Turboiso: Towards Ultrafast and Robust Subgraph Isomorphism Search in Large Graph Databases. *Proceedings of the 2013 ACM SIGMOD International Conference on Management of Data*, 337–348. New York, NY, USA: Association for Computing Machinery.
- He, H., & Singh, A. K. (2008). Graphs-at-a-time: Query Language and Access Methods for Graph Databases. *Proceedings of the 2008 ACM SIGMOD International Conference on*

- Management of Data*, 405–418. New York, NY, USA: Association for Computing Machinery.
- Hong, L., Zou, L., Lian, X., & Yu, P. S. (2015). Subgraph Matching with Set Similarity in a Large Graph Database. *IEEE Transactions on Knowledge and Data Engineering*, 27(9), 2507–2521.
- Kim, H., Choi, Y., Park, K., Lin, X., Hong, S.-H., & Han, W.-S. (2023). Fast Subgraph Query Processing and Subgraph Matching via Static and Dynamic Equivalences. *The VLDB Journal*, 32(2), 343–368.
- Koca, M. B., & Sevilgen, F. E. (2019). A Novel Approach for Subgraph Isomorphism Problem on Bipartite Graphs. *2019 27th Signal Processing and Communications Applications Conference (SIU)*, 1–4.
- Liang, Y., & Zhao, P. (2017). Similarity Search in Graph Databases: A Multi-Layered Indexing Approach. *2017 IEEE 33rd International Conference on Data Engineering (ICDE)*, 783–794.
- Peng, Y., Fan, Z., Choi, B., Xu, J., & Bhowmick, S. S. (2015). Authenticated Subgraph Similarity Searching Outsourced Graph Databases. *IEEE Transactions on Knowledge and Data Engineering*, 27(7), 1838–1860.
- Shang, H., Zhang, Y., Lin, X., & Yu, J. X. (2008). Taming Verification Hardness: An Efficient Algorithm for Testing Subgraph Isomorphism. *Proceedings of the VLDB Endowment*, 1(1), 364–375.
- Tian, Y., & Patel, J. M. (2008). TALE: A Tool for Approximate Large Graph Matching. *2008 IEEE 24th International Conference on Data Engineering*, 963–972.
- Ullmann, J. R. (1976). An Algorithm for Subgraph Isomorphism. *Journal of the ACM*, 23(1), 31–42.